Ministry of Transportation of Quebec
Structural Department

NSERC RESEARCH CHAIR IN FRP REINFORCEMENT FOR CONCRETE STRUCTURES

CONSTRUCTION AND TESTING OF CANADA'S FIRST CONCRETE BRIDGE DECK TOTALLY REINFORCED WITH GLASS FRP BARS: VAL-ALAIN BRIDGE

FINAL REPORT

Prepared by:

Brahim Benmokrane, Ehab El-Salakawy, and Sherif El-Gamal

ISIS-Sherbrooke, Department of Civil Engineering, Faculty of Engineering

University of Sherbrooke, Sherbrooke, Quebec, Canada J1K 2R1
Tel: (819) 821-7758
Fax: (819) 821-7974
E-mail: brahim.benmokrane@usherbrooke.ca

ISIS CANADA
The canadian Network of Centres of Excellence on Intelligent Sensing for Innovative Structures
Le réseau canadian de Centres d'excellence sur les innovations en structures avec système de détection integré

May 2005

ABSTRACT

The Val-Alain Bridge is located in the Municipality of Val-Alain on the Highway 20 East, crosses over the Henri River in Quebec. The bridge is a slab-on-girder type with a skew angle of 20^o. The bridge has four steel girders simply supported over a single span of 48.89 m. The deck slab is a 225-mm thickness concrete slab continuous over three spans of 3.15 m each with an overhang of 1.57 m on each side (measured in the perpendicular direction to axis of the girders). In addition, Type PL-3 concrete bridge barriers totally reinforced with glass FRP bars were used. The concrete deck slab and the bridge barriers were reinforced with sand-coated GFRP composite bars manufactured by a Canadian company (Pultrall Inc., Thetford Mines, Quebec). The Val-Alain bridge is the Canada's first concrete bridge deck totally reinforced with glass FRP bars. The bridge is well instrumented with electrical resistance strain gauges and fibre-optic sensors at critical locations to record internal strain data. Also, the bridge was tested for service performance using calibrated truckloads. Construction details and the results of the first series of live load field tests are discussed. The results reported in this paper provide information about the stress levels in the FRP reinforcement, and steel girders as well as about deck deflection during live load testing.

TABLE OF CONTENTS

LIST OF TABLES

LIST OF FIGURES

1. INTRODUCTION

Corrosion-related bridge deck cracking and spalling constitutes a major problem when measured in terms of rehabilitation costs and traffic disruption (Yunovich and Thompson 2003). Half of Quebec's Department of Transportation's maintenance budget is spent on concrete structures damaged by corrosion of steel. The U.S. National Bridge Inventory lists 40% of the country's 580,000 bridges as either structurally deficient or functionally obsolete. One trillion dollars need to be invested to rehabilitate or replace these bridges (Nystrom 2003). Consequently, the problem has attracted much interest from North American governmental agencies. In 2002, the Federal Highway administration (FHWA) reported that they are focused on advancing FRP composite technology in order to rebuild, rehabilitate, and maintain the infrastructure through their Innovative Bridge Research and Construction (IBRC) (US DOT, 2002). The FHWA established the IBRC with the passage of the Congressional TEA-21 (Twenty-First Century) research funding to investigate the feasibility of using innovative materials in bridge construction in order to develop cost effective materials, reduce maintenance costs, extent service life, improve life-cycle cost efficiency, develop construction and monitoring techniques, and develop design criteria. Federal and provincial governments have both contributed significant amount of funds for research projects that deal with infrastructure and innovative materials (such as the Network of Centres of Excellence ISIS Canada).

Attempts in recent years to address corrosion-related problems have included the development and assessment of alternatives to conventional steel reinforcement, such as epoxy-coated reinforcing steel, nonmetallic reinforcement, and other materials. One of these alternatives, Fibre-reinforced-polymer (FRP) composite reinforcement has been used successfully in many industrial applications and, more recently, has been introduced as concrete reinforcement in bridge decks and other structural elements (Rizkalla et al. 1994 and 1998, Hassan et al. 1999, GangaRao et al. 1997, Japan Concrete Institute 1997, Humar and Razaqpur 2000, Khanna et al. 2000, Tadros 2000, Yost and Schmeckpeper 2001, Steffen et al. 2001, Benmokrane and El-Salakawy 2002, Bradberry 2001, Stone et al. 2001, Nanni and Faza 2002, Huckelbridge and Eitel 2003). These field applications are increasing with the recent publication of several codes and design guidelines for concrete structures reinforced with FRP bars (CAN/CSA-S6-00; ACI 440.1R-01 2001, CAN/CSA-S806-02 2002, ISIS-M03-01 2001).

Through the NSERC Industrial Research Chair in Fiber-Reinforced Polymer Composite Reinforcement for Concrete Infrastructures, a joint effort with the Ministry of Transportation of Quebec (MTQ) was established to develop and implement FRP reinforcement for concrete bridges. After developing and improving these bars and achieving satisfactory laboratory results on concrete deck slab prototypes reinforced with these bars (Benmokrane et al. 2002; El-Salakawy and Benmokrane 2004, El-Gamal et al 2004a,b), the focus shifted to field applications to push the technology forward. These bars were first successfully used in the field in the Wotton Bridge (El-Salakawy et al. 2003).

The Val-Alain Bridge presented herein differs from the previous constructed FRP-reinforced Bridges in that it is located on a federal highway, is larger, and is subject to heavier traffic and a harsher environment. Moreover this project is the Canada’s first full concrete bridge deck totally reinforced with glass FRP bars including the deck slab and the bridge barriers. Once the bridge construction was completed, field testing was conducted to assess service performance under truck wheel loads before the bridge was opened to traffic. Construction details and the results of the first series of live load field tests are discussed herein. The results reported in this paper provide information about the stress levels in the GFRP reinforcing bars and steel girders as well as about the deck deflection obtained from live load testing.

The main objective of these demonstration projects is to implement the technology and to demonstrate its ability to meet all the requirements for concrete construction bridges. Furthermore, assessing the short- and long-term performance of FRP reinforcement and improving/validating current design guidelines under different service loading and environmental conditions stand out as important issues.

2. DESCRIPTION OF THE PROJECT

Val-Alain Bridge is located in the Municipality of Val-Alain on Highway 20 East, over the Henri River in Quebec. The bridge is a slab-on-girder type with a skew angle of 20^{o}. A layout of the bridge is shown in Figure 1.

The bridge has four steel girders simply supported over a single span of 48.89 m (Figure 2,a). The deck slab is a 225-mm thickness concrete slab continuous over three spans of 3.15 m each with an overhang of 1.57 m on each side (measured in the perpendicular direction to axis of the girders). In addition, Type PL-3 concrete bridge barriers totally reinforced with glass FRP bars were used for the first time in Canada. Figure 2b shows the cross-section of the bridge.

The main steel girders are composite with the concrete deck slab using 22-mm diameter × 152 mm long stud connectors as shown in Figure 2c. The steel girders have a constant depth of 2.04 m over the span. The steel beams are supported laterally using 9 cross frames spaced at 6.12 m (Figure 2c). The concrete deck slab and the bridge barriers were reinforced with GFRP composite bars. The GFRP were sand-coated and manufactured by a Canadian company (Pultrall Inc., Thetford Mines, Quebec).

3. MATERIAL PROPERTIES

High performance concrete (Type XIII MTQ) with the composition given in Table 1 was used for the bridge deck. The concrete compressive strength was determined based on the average values from tests performed on three 150×300 mm cylinders, which resulted in an average 28-day compressive strength of 50 MPa. Sand-coated glass FRP bars were used as reinforcement for both bridge deck slab (No. 19, 19.1-mm diameter) and barriers (No. 16, 15.9-mm diameter and No. 19, 19.1-mm diameter). These bars are manufactured by combing the pultrusion process and an in-line coating process for the outside surface. These bars are made from high strength E-glass fibers with a fiber content of 73% in a vinyl ester resin. The mechanical properties of the glass FRP bars used in reinforcing the bridge deck slab and barriers are listed in Table 2.

4. DESIGN OF THE CONCRETE BRIDGE DECK SLABS

Design forces were determined using the flexural design method specified in the Canadian Highway Bridge Design Code (CSA-S6-00, section 8). The design moments were based on a maximum wheel load of 87.5 kN (CL-625 Truck). The design service load of the deck slabs was taken as $1.4 \times 0.9 \times 87.5 = 110.25$ kN, where 1.4 is the impact coefficient (clause 3.8.4.5.1), and 0.9 is the live load combination factor (clause 3.5.1). While the design factored load was taken as $1.4 \times 1.7 \times 87.5 = 208.25$ kN, where 1.7 is the live load factor (clause 3.5.1).

The deck slab was designed based on serviceability criteria. The crack width and allowable stress limits were the controlling design factors. The Ministry of Transportation of Quebec (MTQ) has selected to limit the maximum allowable crack width to 0.5 mm and the stresses in the GFRP bars to 30 and 15% of the ultimate strength of the material under service and sustained loads, respectively. Based on this design approach, the bridge deck slab was entirely reinforced with two identical reinforcement mats using No. 19 glass FRP bars. For each reinforcement mat, No. 19 GFRP bars spaced at 125 and 185 mm in the transverse and longitudinal directions were used, respectively. A 38 mm top and bottom clear cover was used. Figure 3 shows the reinforcement details of the deck slab.

Additional No.19@250 mm GFRP bas were placed in the top transverse layer at the two cantilevers, as well as to the top longitudinal layer at the ends of the deck slab as shown in Figure 4. There were no splices of the GFRP bars in the transverse direction. However three splices with a splice length of 800 mm (about 40 times the bar diameter) were used in the longitudinal direction. The reinforcement configurations are shown in Table 3.

5. INSTRUMENTATION

The bridge was well instrumented at critical locations to record internal temperature and strain data. Instrumentation was distributed in two sections on the bridge, namely, Sections 1 and 2 at mid-span and near the quarter span (between two cross diaphragms) of the bridge, respectively, (Figure 5a). Fabry-Perot fibre optic sensors (FOS) and electrical resistance strain gauges were glued on transverse reinforcing bars at locations of expected maximum stresses (on top of and between support girders for top and bottom bars, respectively) and on top longitudinal reinforcement located on the top of girder B at section 1 (Figure 5a,b). The locations of the gauges were identical for the two instrumented sections. However, electrical gauges were used at all locations. While, FOS gauges were used only at locations T1, B1, T2, B2 and T10, (Figure 5a) in section 1.

Furthermore, ten electrical resistance strain gauges were glued on the surface of steel girders (Section 1) to measure strains at the web and bottom flanges. Two thermocouples were embedded in the concrete at the top and bottom of Sections 2 to measure temperature changes. The objective of using FOS gages is to allow for the long-term monitoring of the bridge, while electrical strain gages have been selected only for the purpose of the short-term testing reported in this report. Figure 5c shows fibre-optic sensors glued to the surface of the FRP bars. In addition, slab and girder deflection was measured with a system of rulers (located in Sections 1) as shown in Figure 5d. This instrumentation acquires data and provides for the long-term monitoring of bridge behaviour under service and environmental conditions.

6. BRIDGE CONSTRUCTION

The construction of the bridge started on July 2004. Due to the light weight of GFRP bars, more FRP bars could be handled in less time as shown in Figure 6a. Continuous plastic supports were placed under the bottom reinforcement parallel to the longitudinal direction at 0.75 m intervals to maintain a clear concrete cover of 38 mm at the bottom (Figure 6b). Individual plastic chairs, however, were spaced at 0.75 m intervals in both directions to support the top FRP bars and to maintain a clear top concrete cover of 38 mm as shown in Figure 6c. In addition, circular chairs were connected to the barriers reinforcement to maintain a side concrete cover of 75 mm as shown in Figure 6d.

The FRP bars were spliced only in the longitudinal directions using a splice length of 800 mm (about 40 times the bar diameter) as shown in Figure 6e. The additional GFRP bars at the overhang placed in between the continuous transverse top reinforcement were extended to a distance of 1.4 m into the adjacent span. Type PL-3 barriers reinforced with bent glass FRP bars were used for this bridge as shown in Figure 6f. The FRP bars withstood all on-site handling and placement problems. The FRP reinforcement in the deck slab before concrete casting is shown in Figure 6g. The bridge deck slab was cast on October 7, 2004, then the concrete barrier walls were cast one week later.

Figure 6h and 6i show the bridge during and just after casting of concrete. After the concrete deck was cured for two weeks, it was paved with a 65-mm thick layer of asphalt. The bridge was ready for testing at the end of October 2004. Figure 6j shows the bridge just after the completion of the construction.

7. STATIC AND DYNAMIC TESTING OF THE BRIDGE

The bridge was tested on October 30, 2004 for service performance as specified by the new CHBDC (CAN/CSA-S6-00)[1] using two four-axle trucks. Trucks No.1 and No.2 had loads of 65 kN and 54 kN on the first front axle, 71 kN and 64 kN on the second front axle and approximately 96 kN and 103 kN per each back axle, respectively. Figure 7 shows the complete description of the trucks. The two trucks were used simultaneously to carry out the rest of the tests described below. The bridge was tested under static and dynamic loads using the two truckloads described. Two data-acquisition systems were installed underneath the bridge to collect data from electrical and FOSs gauges during testing. During all static tests, the deflections of the concrete slab and steel girders were measured using a system of rulers and theodolites.

7.1 Static Test

Based on Finite Element Analysis of the bridge deck slab, four paths in the direction of traffic (A, B, C, and DE) were marked on the bridge (Figure 8a) to give the maximum moments of the deck slab. The first three paths (A, B, and C) were chosen to give the maximum positive moments. The fourth path (DE) was chosen to give the maximum negative moments. Four stations (truck stops) were also marked along the longitudinal direction of the bridge at selected positions to match the instrumentation positions (Figure 8b). The first stage of the test was carried out using Truck No. 1 (paths A, B, and C) to record 12 readings (3 paths × 4 stations) for each gauge and deflection ruler. In the second stage of the test, the two trucks were used (path DE) to record a total of 4 readings for each gauge and deflection ruler. Readings were recorded at each truck station when the midpoint of the truck's third axle (first rear axle) was directly over the station. Figure 9 shows the trucks on the bridge during testing.

7.2 Dynamic Test

Dynamic testing was carried out using the same two calibrated trucks described for static testing. The trucks followed the same four paths in the traffic direction, as shown in Figure 8a. The trucks traveled, either separately or simultaneously (two trucks behind each other, or two trucks beside each other), at two different speeds: 5 km/h and 50 km/h.

Truck No. 1 traveled over the first three paths (A, B, and C) at a speed of 5 km/h, while the two trucks (beside each other) travelled over path DE at the same speed (total of 4 paths). At a speed of 50 km/h, the two trucks (behind each other) traveled over the first three paths (A, B, and C), while the two trucks (beside each other) travelled over the last path (path DE) (total of 4 tests). The data-acquisition system was adjusted to a rate of 200 readings/sec.

8. STATIC TESTING RESULTS

8.1 Electrical Resistance Strain Gauges Results: Strains in FRP reinforcements

Figures 10 and 11 show the maximum tensile strains measured in the bottom and top transverse FRP reinforcing bars versus truckload position on the bridge, respectively. As a result of the truck paths, the single truck was expected to produce maximum strain in the bottom FRP bars and the two trucks together were expected to produce maximum strain in the top FRP bars. The maximum measured tensile strain in the bottom reinforcement was recorded in gauge B2 (Path B) as expected. The maximum measured strain was 57 micro-strains (corresponding to a tensile stress of 2.51 MPa) as shown in Figure 10. The maximum measured tensile strain in the top reinforcement was recorded in gauge T3 (Path DE, two trucks), which was 22 micro-strains (corresponding to a tensile stress of 0.97 MPa) as shown in Figure 11.

The maximum compressive strain measured in the top longitudinal reinforcement versus truckload position on the bridge was recorded in gauge T9 (Path DE). The maximum measured compressive strain was 30 micro-strains (corresponding to a compressive stress of 1.32 MPa) as shown in Figure 12.

Figures 13 to 20 show the measured reinforcement strains at each gauge for different paths. It can be noted that the single truck (Paths A, B and C) produced the maximum strains in the bottom reinforcement; however the two trucks (Path DE) produced the maximum strains in the top reinforcement.

8.2 FOS Results versus Electrical Resistance Strain Gauges Results

Similar strain readings were obtained from the fibre-optic sensors and the electrical resistance strain gauges. Figure 21 compares the measured strains in the FRP top reinforcement using fibre-optic sensors and electrical resistance strain gauges glued at identical positions on the FRP bars. The strains measured by the electrical resistance strain gauges, however, little bit higher than that measured by the fibre-optic sensors due to the location of the instrumented FRP bars. The FRP bar instrumented with electrical resistance strain gauges was exactly under the truck station; however, the FRP bar instrumented with FOS was 125 mm (the spacing between the transverse reinforcement) away from the truck station.

8.3 Strains in Steel Girders

Figures 22 to 25 show the measured strains in the bottom flange of steel girders with respect to truckload positions on the bridge for different paths. It can be noted that the maximum strains were recorded in the two middle girders B and C (Figures 23 and 24) due to path DE (two trucks) as expected. The maximum measured strain was 87 micro-strains which correspond to stress of 17.4 MPa. The distribution of measured strains in girder B with respect to truckload positions on the bridge for path DE is shown in Figure 26. Figure 27 shows the distribution of strains at the mid span of girder B (Path DE, station 2 at the mid span of the bridge). From the two Figures, it can be noted that the maximum strain was recorded at the bottom flange of the girder. Moving to the top of the girder decreases the tensile strains linearly as expected.

Figure 28 shows the distribution of the maximum tensile strains in the steel girders measured at the midspan of the bridge (Section 1) due to truckloads at different paths. Note that the truckloads are not evenly distributed over the steel girders. The girder closer to the truckloads carries more loads than the one away from it. In addition, for path DE (two trucks) the strains in the girders were symmetric due to the symmetric of the loading of the girders.

8.4 Deflection Measurements

During static testing, deflection of concrete slabs and steel girders was measured with a theodolite using a system of rulers installed at the mid-span of the bridge (Section 1) as shown in Figure 29. The maximum measured deflections were recorded for the two trucks traveling on Path DE. With that path the measured peak deflection of the steel girder B and C was 14.0 mm and 12.0 mm, respectively, as shown in Figure 30.

The deflection of the concrete deck slab was calculated by subtracting the measured value at the considered position on the slab from the average of the measured values at the two steel girders adjacent to that position. These maximum-calculated values were less than 3 mm and were obtained with the two trucks traveling on path DE as shown in Figure 31.

9. DYNAMIC TEST RESULTS

9.1 Strains in FRP Reinforcement

Figures 32 to 39 show the maximum tensile strains measured in top and bottom FRP reinforcement against time for different paths at speeds of 5 and 50 km/h. It can be noted that the maximum measured tensile strain was recorded in the bottom reinforcement (gauge B2) due to one truck traveling over path B (the same gauge and path as in the static test) as shown in Figures 34 and 35. The maximum tensile strain was 53 and 48 micro-strain for speeds of 5 km/h and 50 km/h, respectively. Compared to the static test (57 micro-strain), the maximum tensile strains decreased by about 7% and 16% by increasing speeds to 5 km/h and 50 km/h, respectively.

For the top reinforcement, the maximum tensile strains were also recorded in the same gauge for the same path as recorded in the static test (gauge T3, Path DE) as shown in Figures 38 and 39. The maximum tensile strain was 22 micro-strain at a speed of 5 km/h (the same as in the static testy), however it decreased to 20 micro-strain at a speed of 50 km/h.

Figures 40 and 41 show the maximum measured compressive strains in FRP reinforcement (gauge T9, Path DE) at speeds of 5 and 50 km/h., respectively. The maximum compressive strains were 39 micro-strain and 34 micro-strain for speeds 5 and 50 km/h, which are higher than the maximum compressive strain due to the static test (30 micro-strain) by about 30% and 13%, respectively.

9.2 Strains in Steel Girders

Figures 42 and 43 show the maximum tensile strains measured at the mid span of the steel girders against time for the two trucks traveling on Path DE at speeds of 5 and 50 km/h., respectively. It can be notes that the maximum strains were recorded in the two middle girders B and C. The maximum measured strain was the same for the two speeds (85 micro-strain) that corresponds to a stress of 17 MPa. It can be noted that the maximum measured strains due to the dynamic test were almost the same as that measured due to the static test (87 micro-strain).

10. CONCLUSIONS

This report presents the construction details and test results for the Val-Alain Bridge located on Highway 20 East concrete bridge deck reinforced with glass FRP reinforcing bars. Based on the construction details and the results of the first field-loading test, the following conclusions can be drawn.

1. No obstacles to construction were encountered due to the use of the GFRP bars for the deck slab and bridge barriers (Type PL-2). The GFRP bars withstood normal on-site handling and placement problems.
2. During the entire test, the maximum tensile strain in GFRP bars was 57 micro-strains. This value is less than 0.4 % of the ultimate strain of the GFRP pars. This result suggests that the CHBDC flexural design method overestimates the calculated design moments (service and ultimate).

3. Strain readings obtained from fibre-optic sensors glued to reinforcing bars were very similar to those obtained from the electrical resistance strain gauges glued at identical positions on the reinforcing bars.
4. Bridge-deck and slab deflections were well below CHBDC and AASHTO allowable limits. During all stages of testing, the maximum measured deflections for steel girders and concrete slabs were 14 and 3 mm, respectively.
5. The bridge presented in this report was designed according to the flexural design method. In the future, other bridges will be designed according the empirical design method then they will be tested in the field. The results from field testing of these bridges will help in reducing the required amount of GFRP reinforcing bars in the deck slab. This will result in more economic design to offset the initial high cost of GFRP bars.

ACKNOWLEDGEMENT

The authors thank the Ministry of Transportation of Quebec (Department of Structures) for collaboration in this project. Our thanks are also extended to Pultrall Inc. (Thetford Mines, Québec), Construction Génix Inc. (Québec, Québec), Roctest Ltd. (St-Lambert, Québec) and Avensys Inc. (Montréal, Québec). The Natural Science and Engineering Research Council of Canada, NSERC, (Ottawa, Ontario), the Fonds Québécois sur la Recherche en Nature et en Technologie (Qébec, Québec), and ISIS-Canada, Network of Centres of Excellence are also acknowledged for partial funding.

11. REFERENCES

AASHTO. (1996). “Standard specifications for design of highway bridges.” American Association of State Highway and Transportation Officials, Washington, D.C.

ACI 440.1R-01. (2001). “Guide for the design and construction of concrete reinforced with FRP bars.” *American Concrete Institute*, Farmington Hills, Michigan, 41p.

Bakht, B., and Lam, C. (2000). “Behaviour of transverse confining systems for steel-free deck slabs.” *ASCE Journal of Bridge Engineering*, **5**(2), 139–147.

Bradberry, T.E. (2001). “Concrete Bridge Decks Reinforced with Fiber Reinforced Polymer Bars.” Transportation Research Record 1770, Transportation Research Board, National Research Council, Washington, DC, 94-104.

Benmokrane, B., Zhang, B., Laoubi, K., Tighiouart, B., and Lord, I. (2002). “Mechanical and bond properties of new generation of carbon fiber reinforced polymer reinforcing bars for concrete structures." *Canadian J. of Civil Engrg*, 29(2), 338-343.

CAN/CSA-S6-00. (2000). “Canadian highway bridge design code.” *Canadian Standards Association (CSA) International*, Rexdale, Toronto, Ontario, Canada, 734 p.

CSA S806–02. (2002). “Design and construction of building components with fiber reinforced polymers.” *Canadian Standards Association (CSA) International*, Rexdale, Toronto, Ontario, Canada,177 p.

El-Gamal, S.E., Elsalakawy, E.F., and Benmokrane, B. (2004)a. “Behaviour of FRP Reinforced Concrete Bridge Decks under Concentrated Loads,” Proceedings of the 4th International Conference on Advanced Composite Materials in Bridges and Structures, Calgary, Alberta, July 20 – 23, 2004.

El-Gamal, S.E., Elsalakawy, E.F., and Benmokrane, B. (2004)b. “Behaviour of Bridge Decks Slabs Reinforced with Glass FRP Composite Bars,” Proceedings of the 32nd Canadian Society of Civil Engineering Annual Conference, Saskatoon, Saskatchewan, Canada, Juin, 2004.

El-Salakawy, E.F. and Benmokrane, B. (2002). “Concrete bridge deck slabs reinforced with using FRP composite bars: Magog Bridge on Highway 55.” *Internal Report*, Department of Civil Engineering, University of Sherbrooke, November, 49 p.

El-Salakawy**,** E.F. and Benmokrane, B. (2004). “Serviceability of concrete bridge deck slabs reinforced with FRP composite bars.” *ACI Structural Journal*, 101(5), Sept.-Oct., 593-604.

El-Salakawy, E.F., Benmokrane, B., and Desgagné, G. (2003). “FRP composite bars for the concrete deck slab of wotton bridge.” *Canadian J. of Civil Engrg,* 30(5), 861-870.

El-Salakawy, E.F., Benmokrane, B., and Desgagné, G. (2004). “Reply to discussion by Bakht et al. on FRP composite bars for the concrete deck slab of Wotton bridge.” *Canadian J. of Civil Engineering,* 31(3), 532-533.

Fang, I. K., Worley, J. Burns, N. H., and Klingner, R. E. (1990). "Behavior of isotropic reinforced concrete bridge decks on steel girders." *ASCE, Journal of Composites of Construction*, 116(3), 659-678.

GangaRao, H.V.S., Thippesway H. K., Kumar S. V., and Franco J.M. (1997). “Design, construction and monitoring of the first FRP reinforced concrete bridge deck in the United States.” *Proceedings of the third International Symposium (FRPRCS 3) on Non-Metallic (FRP) Reinforcement for Concrete Structures,* Sapporo, Japan, vol. 1, pp. 647-656.

Hassan, T., Rizkalla, S., Abdelrahman, A., and Tadros, G. (1999). “Design recommendations for bridge deck slabs reinforced by fiber reinforced polymers.” *Proceedings of the Fourth International Symposium on Fiber Reinforced Polymers Reinforcement for Concrete Structures, FRPRCS-4*, ACI-SP-188, Baltimore, USA, 313-323.

Hewitt, B.E. and Batchelor, B., (1975). "Punching Shear Strength of Restrained Slabs." *ASCE Journal of Structural Division*, 101(ST9), Sept., 1837- 1853.

Huckelbridge, A. A., and Eitel, A. K. (2003). “Preliminary performance observations for FRP reinforced concrete bridge deck.” *American Concrete Institute (ACI) Special Publication*, Field Applications of FRP Reinforcement: Case Studies, Farmington Hills, Michigan, SP-215-7, 121-138.

Humar, J. and Razaqpur, G., editors. (2000). “Advanced Composite Materials in Bridges and Structures.” *Proceeding of the Third International Conference*, Ottawa, Ontario, Canada, 876p.

ISIS-M03-01. (2001). “Reinforcing concrete structures with fiber reinforced polymers.” *The Canadian Network of Centers of Excellence on Intelligent Sensing for Innovative Structures*, ISIS Canada, University of Winnipeg, Manitoba, 81 p.

Japan Concrete Institute, editor. (1997). “Non-metallic (FRP) reinforcement for concrete structures.” *Proceeding of the third International Symposium (FRPRCS-3),* Sapporo Japan, Vol. 1, 728p.

Khanna, S., Mufti, A., and Bakht, B. (2000). “Experimental investigation of the role of reinforcement in the strength of concrete deck slabs.” *Canadian J. of Civil Engrg,* 27(5), 475-480.

Kuang, J. S. and Morely, C. T., (1992). "Punching shear behavior of restrained reinforced concrete slabs." *ACI Structural Journal*, 89(1), Jan-Feb., 13-19.

Nanni, A. and Faza, S. (2002). “Designing and constructing with FRP bars: an emerging technology.” *American Concrete Institute ACI Concrete International*, 24(11), 53-58.

Rizkalla, S. and Tadros, G. (1994). “First smart bridge in Canada.” *American Concrete Institute ACI Concrete International*, 16(6), 42-44.

Rizkalla, S., Shehata, E., and Abdelrahman, A. (1998). “Design and construction of a highway bridge reinforced for shear and prestressed by CFRP.” *American Concrete Institute Seminar* on Field Applications of FRP Reinforcement to Concrete: Part I and Part II, Atlanta, Georgia, 5p.

Steffen, R.E., Trunfio, J.P., and Bowman, M.M. (2001). “Performance of a bridge deck reinforced with CFRP grids in rollinsford, New Hampshire, USA.” *Proceedings, CCC 2001, FRP Composites in Construction*, Porto, Portugal, Oct. 10-12, J. Figueiras, L. Juvandes and R. Furia, Eds., 671-676.

Stone D., Nanni, A., and Myers, J.J. (2001). “Field and laboratory performance of FRP bridge decks.” *Proceedings, CCC 2001, FRP Composites in Construction*, Porto, Portugal, Oct. 10-12, J. Figueiras, L. Juvandes and R. Furia, Eds., pp. 701-706

Tadros, G. (2000). “Provisions for using FRP in the Canadian highway bridge design code.” *American Concrete Institute ACI Concrete International*, 22(7), 42-47.

US DOT FHWA. (2002). “FRP Composite Bridge Technology.” *US DOT FHWA, Feb. 4*, *www.fhwa.dot.gov/bridge/frp/frpintro.htm* (Aug. 19, 2002)

Yost, J.R., and Schmeckpeper, E.R. (2001). "Strength and serviceability of FRP grid reinforced bridge decks.” *J. of Bridge Engrg*, ASCE, 6(6), 605-612

Yunovich, M., and Thompson, N. (2003). "Corrosion of highway bridges: economic impact and control methodologies." *American Concrete Institute, ACI Concrete International*, 25(1), 52-57.

Table 1 – Composition of used concrete

Concrete Type	Cement content (kg/m^3)	Water/Cement Ratio	Aggregate size (mm)	Air content (%)
XIII (BHP)	410	0.34-0.38	5-14	5-8

Table 2 - Properties of FRP reinforcing bars

Bar Type	Diameter (mm)	Area (mm^2)	Modulus of Elasticity (GPa)	Tensile Strength (MPa)	Ultimate Strain (%)
GFRP (No. 19)	19.0	283	44.0	637 ± 15 [592] *	1.37 ± 0.03 [1.28] *

*Guaranteed value

Table 3- Concrete deck slab reinforcement

Rein. Type	Bottom Reinforcement		Top Reinforcement		Overhang
	Transverse	Longitudinal	Transverse	Longitudinal	Transverse
GFRP (ρ)	No.19@125 (1.348 %)	No.19@185 (0.91 %)	No.19@125 (1.348 %)	No.19@185 (0.91 %)	No.19@125 + No.19@250 (additional) (2.02 %)

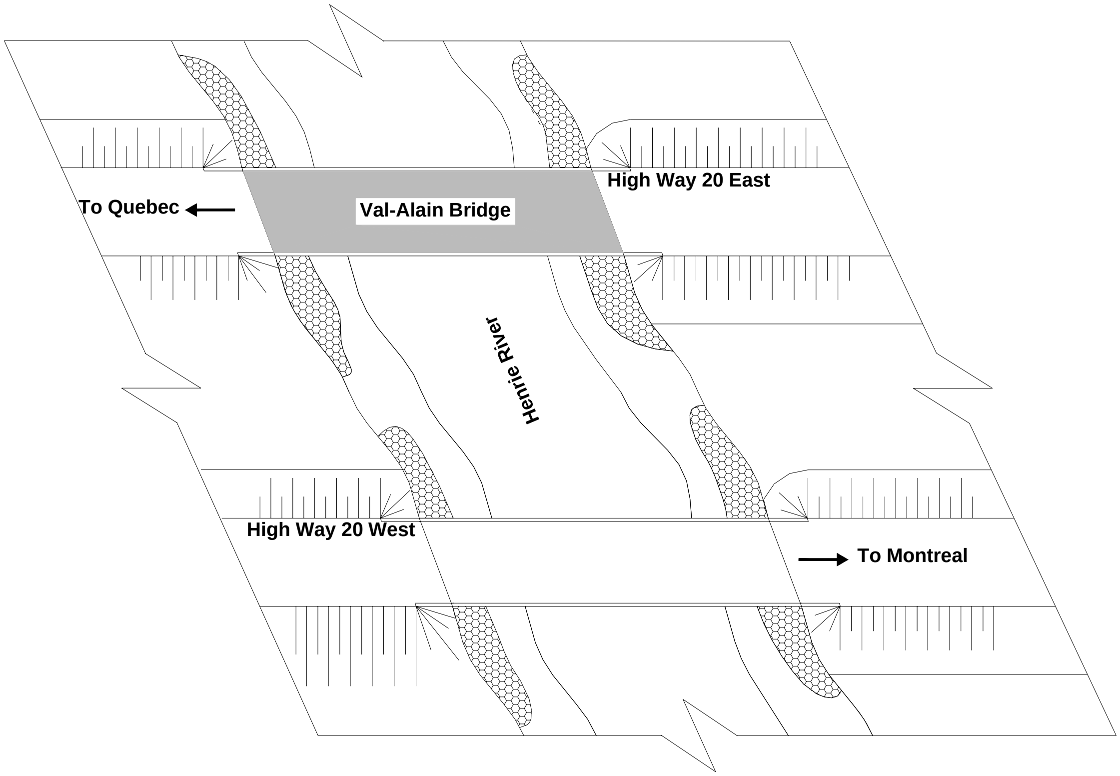

(a) plan view

(b) photo for the bridge during construction

Figure 1 - Layout of Val-Alain Bridge

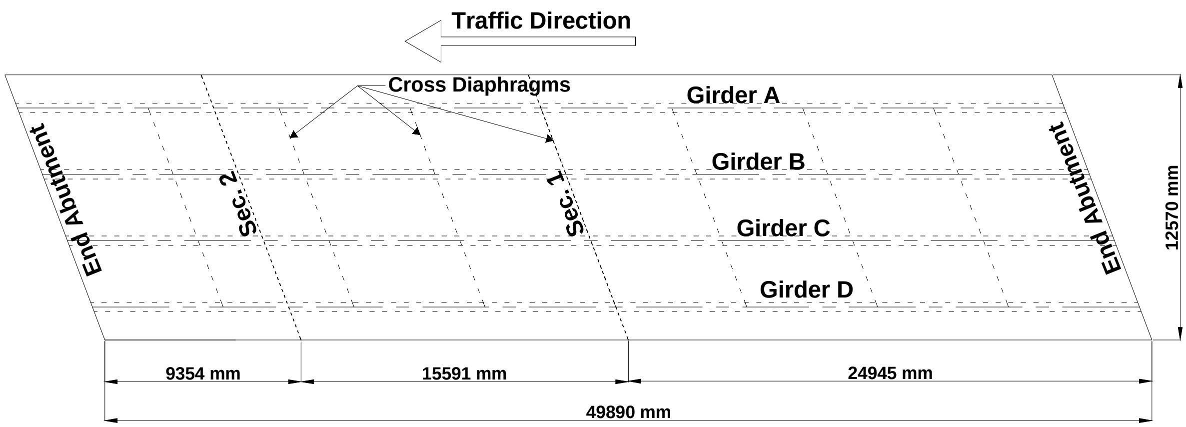

(a) plane of the bridge

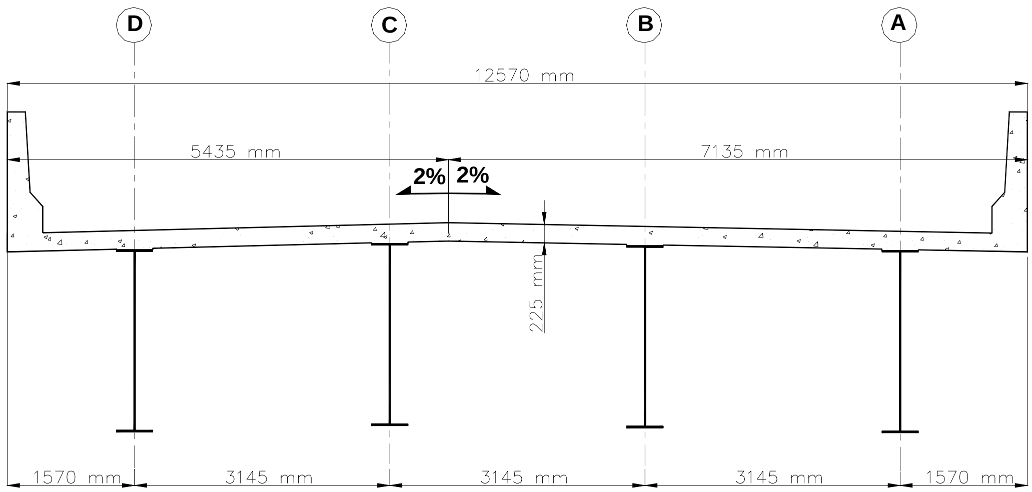

(b) cross-section of the bridge

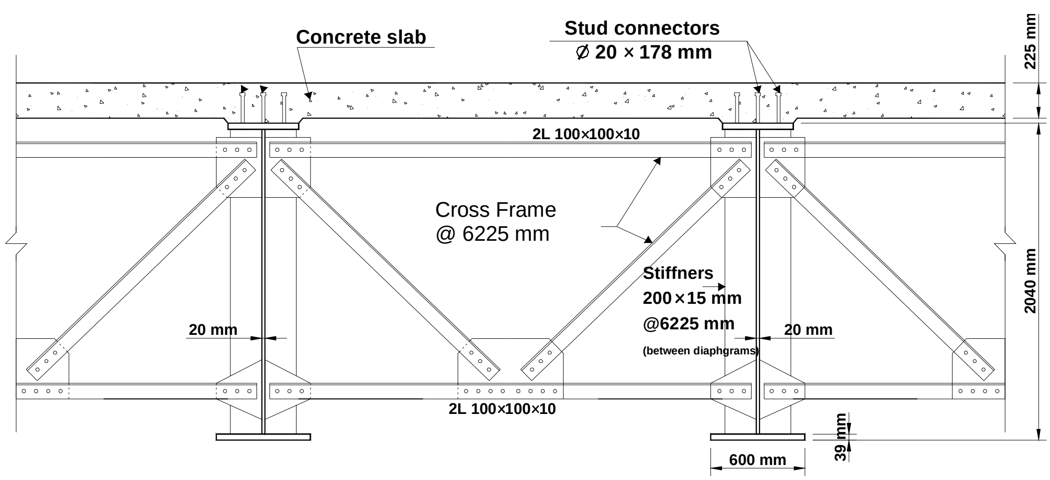

(c) details of the supporting girders and cross diaphragms

Figure 2 - Dimensions of Val-Alain Bridge

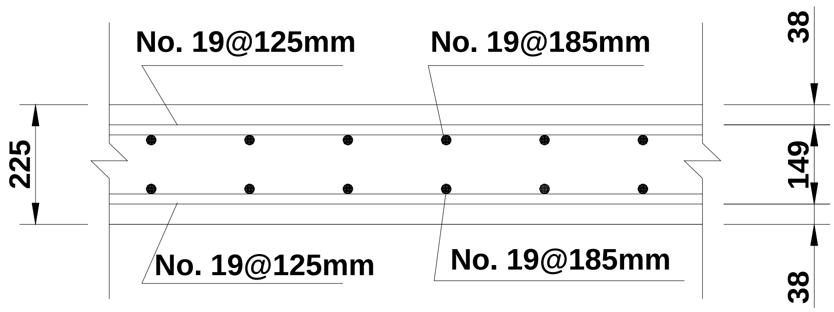

Figure 3 - Slab Reinforcement (cross-section perpendicular to main girders)

(a) additional reinforcement for cantilevers

(b) additional reinforcement at the ends

Figure 4 - Additional GFRP reinforcement for cantilevers and slab ends

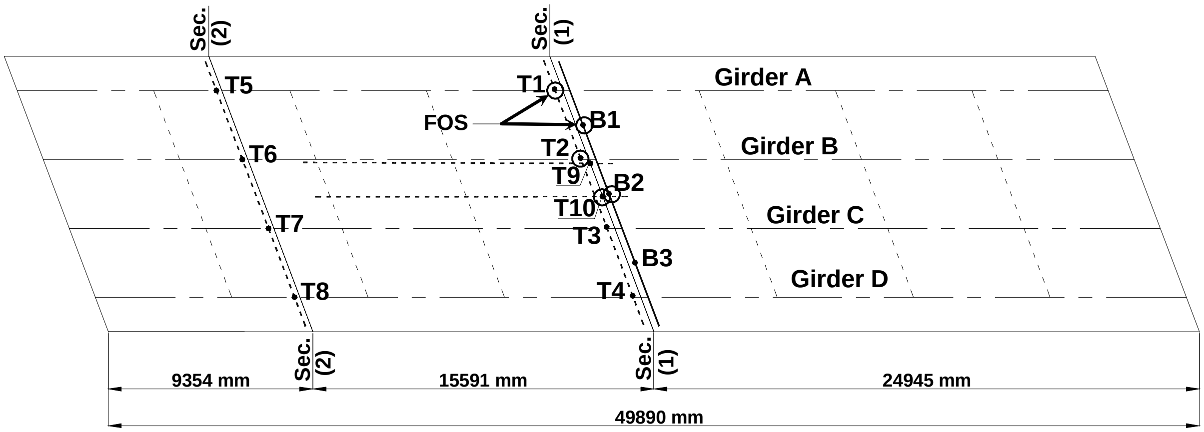

(a) schematic drawing for the locations of reinforcement strain gauges (plan view)

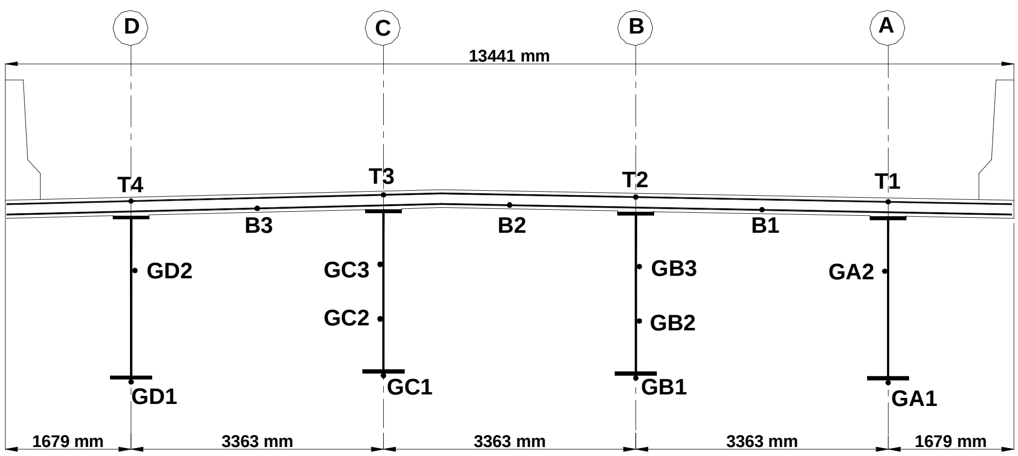

(a)

(b) schematic drawing for the locations of reinforcement and girders strain gauges (section 1, at the mid span of the bridge)

(c) electrical and FOS strain gauges (d) slab and girder system of rulers

Figure 5 – Bridge instrumentation

(a) carrying of GFRP bars

(b) continuous chairs in the longitudinal direction

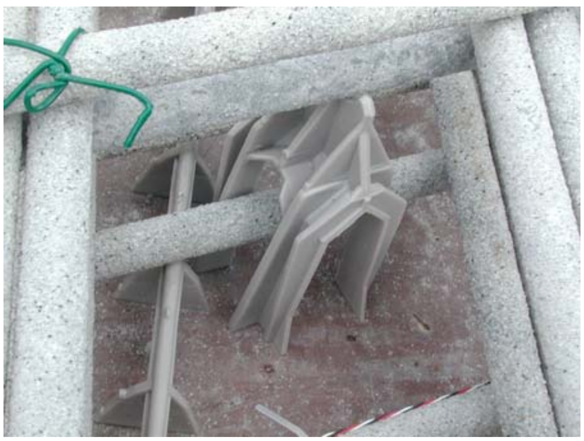

(c) individual chairs (for top reinforcement)

(d) barriers chairs

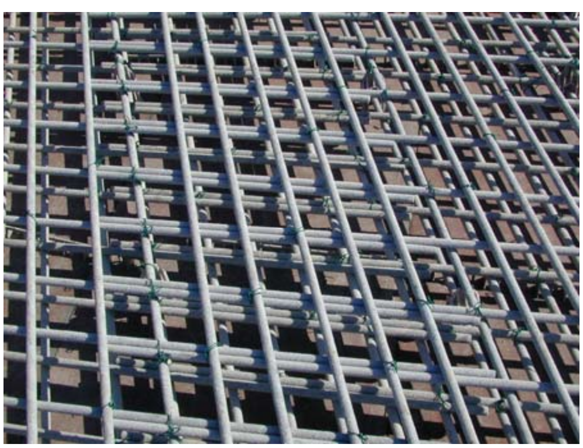

(e) splice in the longitudinal reinforcement

(f) reinforcement of the bridge barriers

Figure 6 - The bridge construction

(g) bridge deck before casting

(h) bridge deck during casting

Figure 6 (cont.) - The bridge construction

(i) bridge deck just after casting

(j) the bridge after the construction

Figure 6 (cont.) - The bridge construction

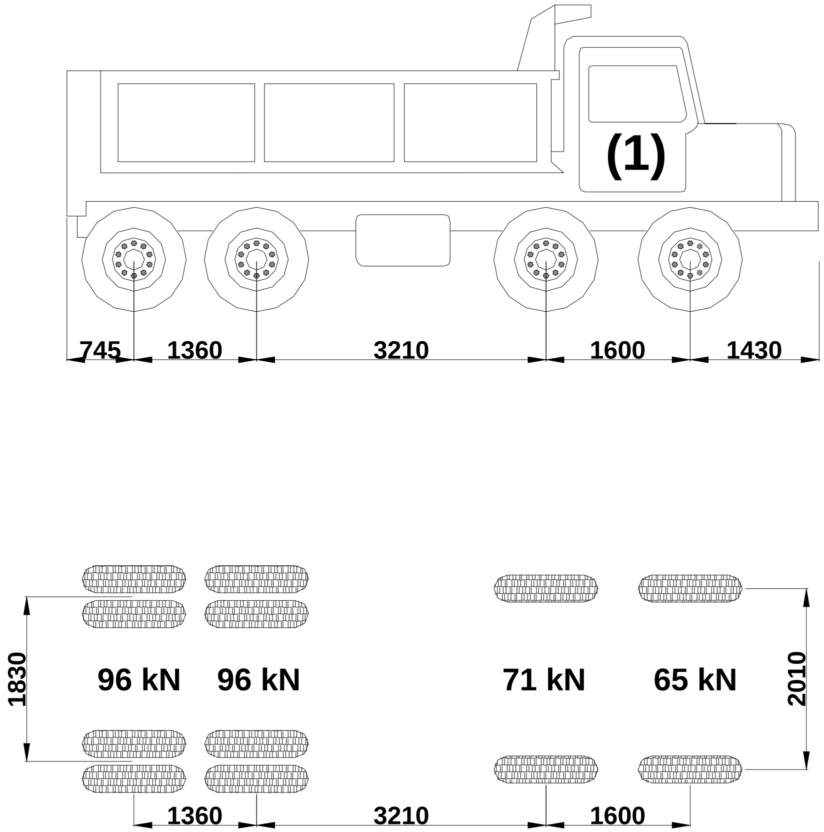

Truck (1)

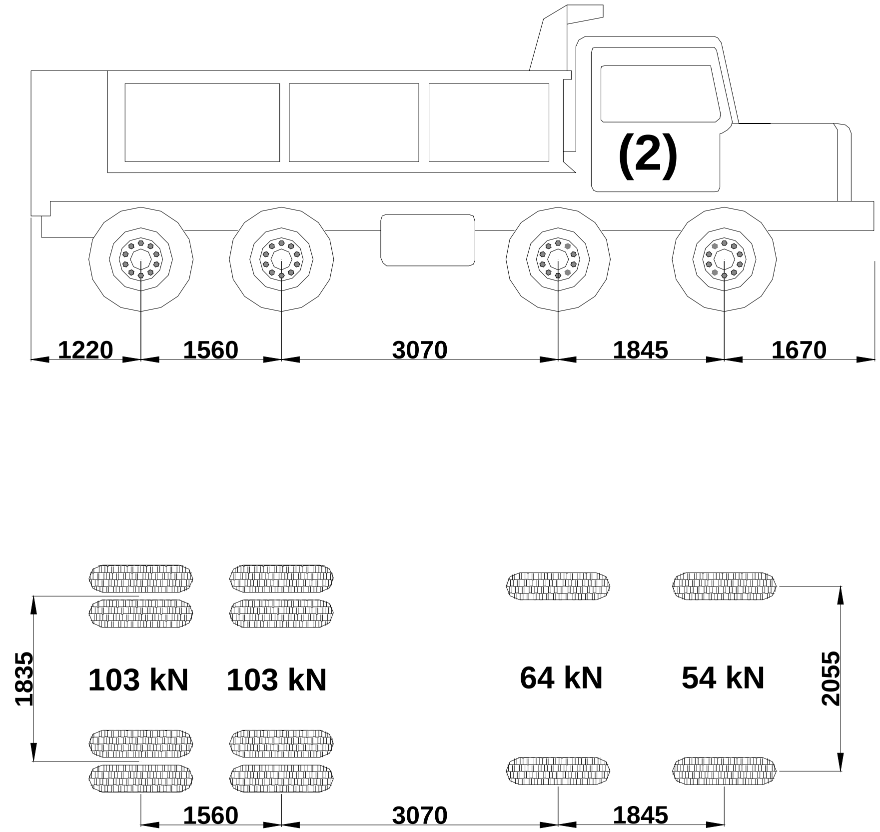

Truck (2)

Figure 7 – Truck loads

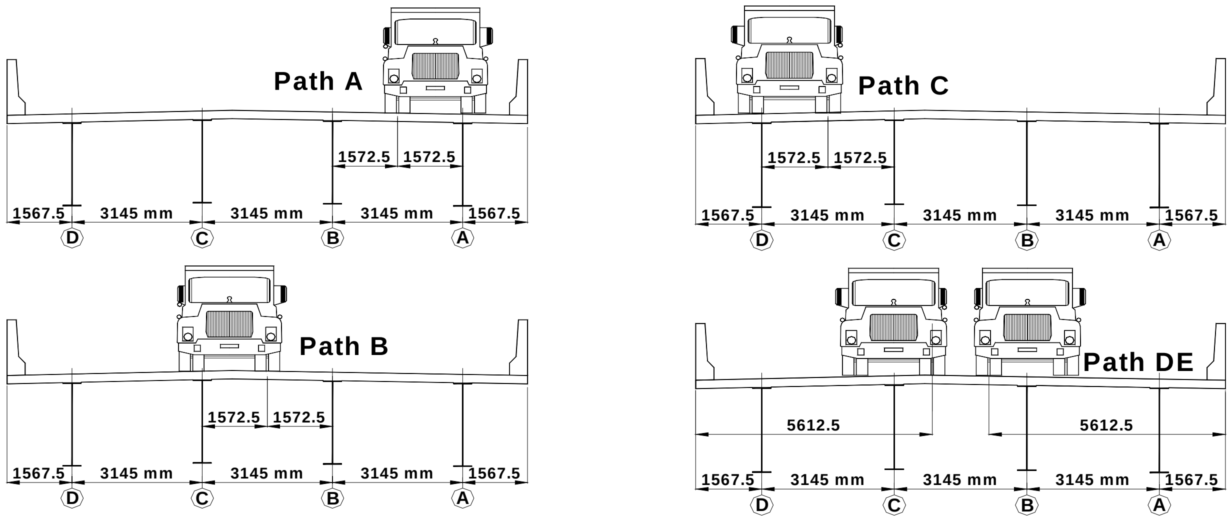

(a) Paths

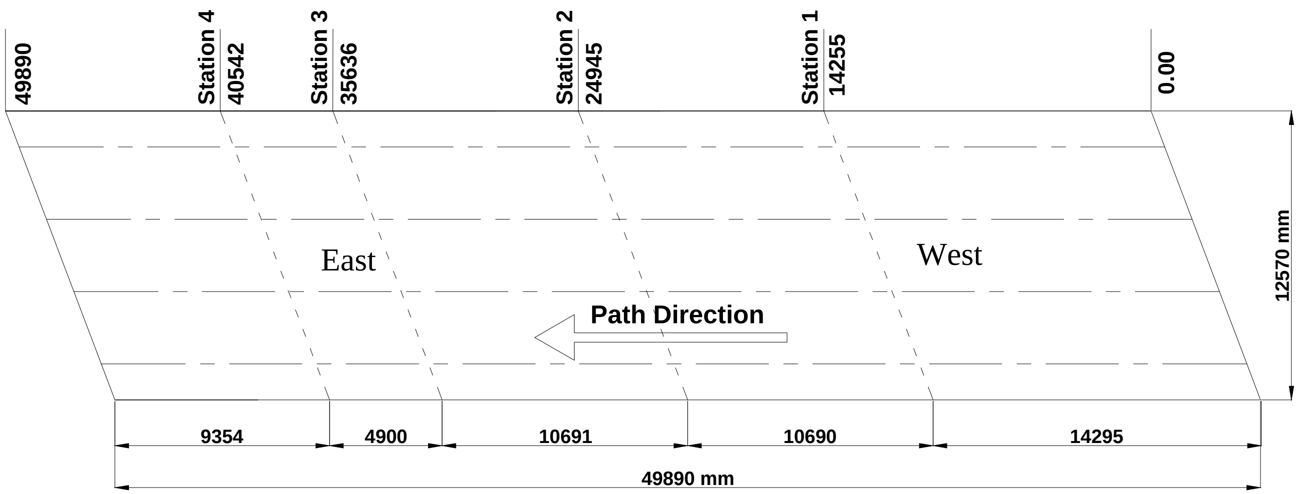

(b) Stations

Figure 8 – Paths and stations of the trucks during testing

Figure 9 – Trucks during testing (Path DE)

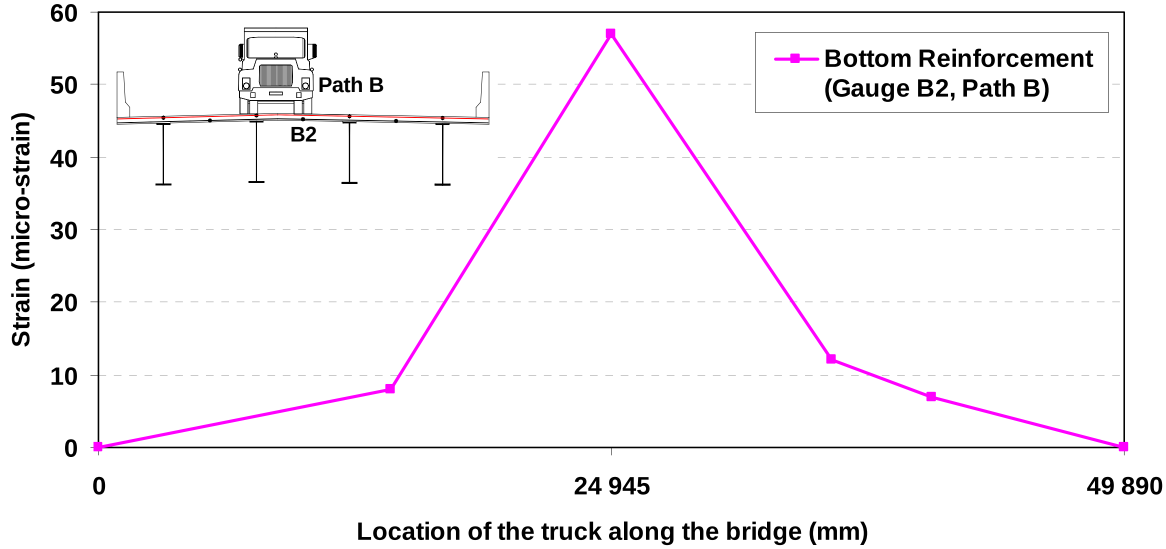

Figure 10 - Maximum tensile strains in bottom transverse reinforcement (gauges B2, path B)

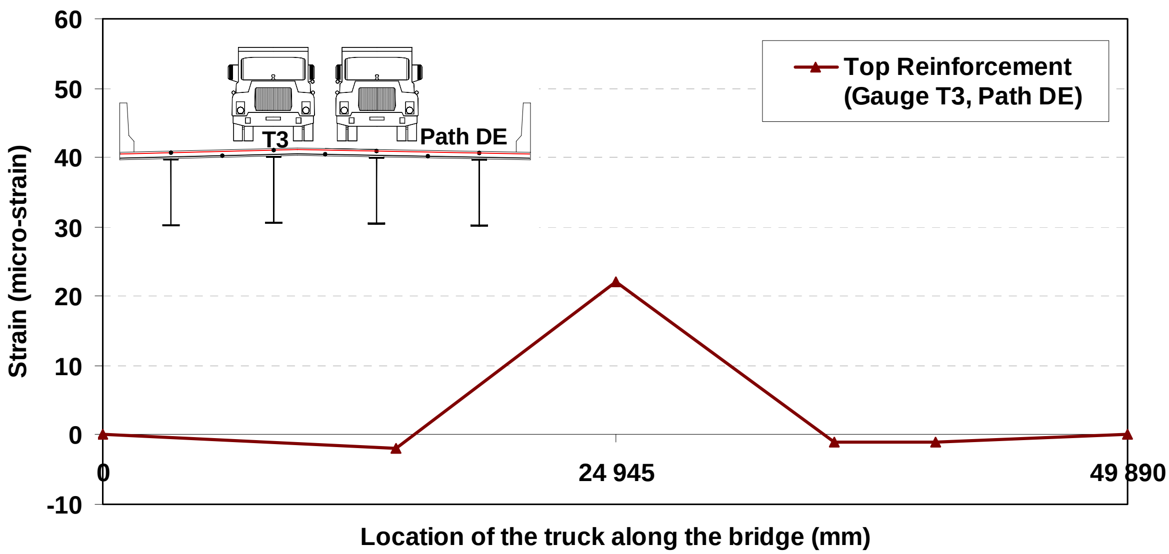

Figure 11 - Maximum tensile strains in top transverse reinforcement (gauges T3, path DE)

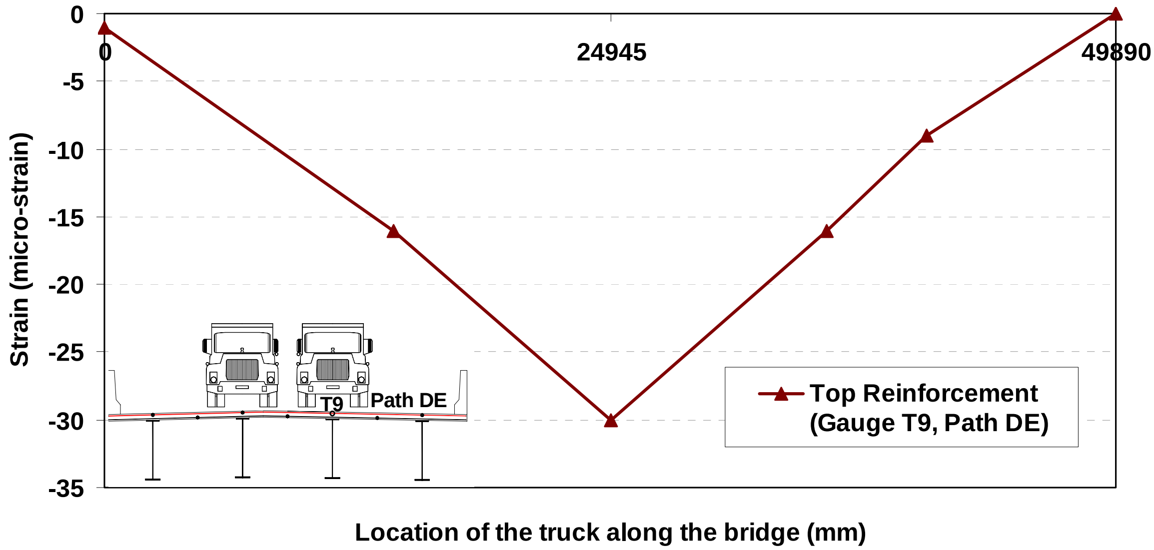

Figure 12 - Maximum compressive strains in top longitudinal reinforcement (gauges T9, path DE)

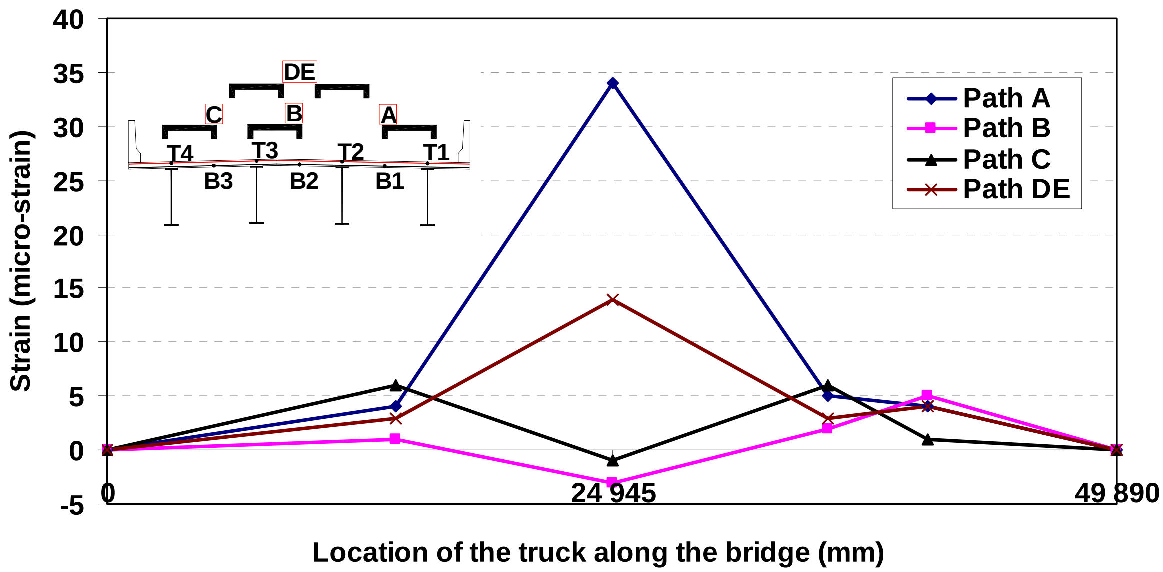

Figure 13 – Measured strains in bottom transverse reinforcement for different paths (Gauge B1)

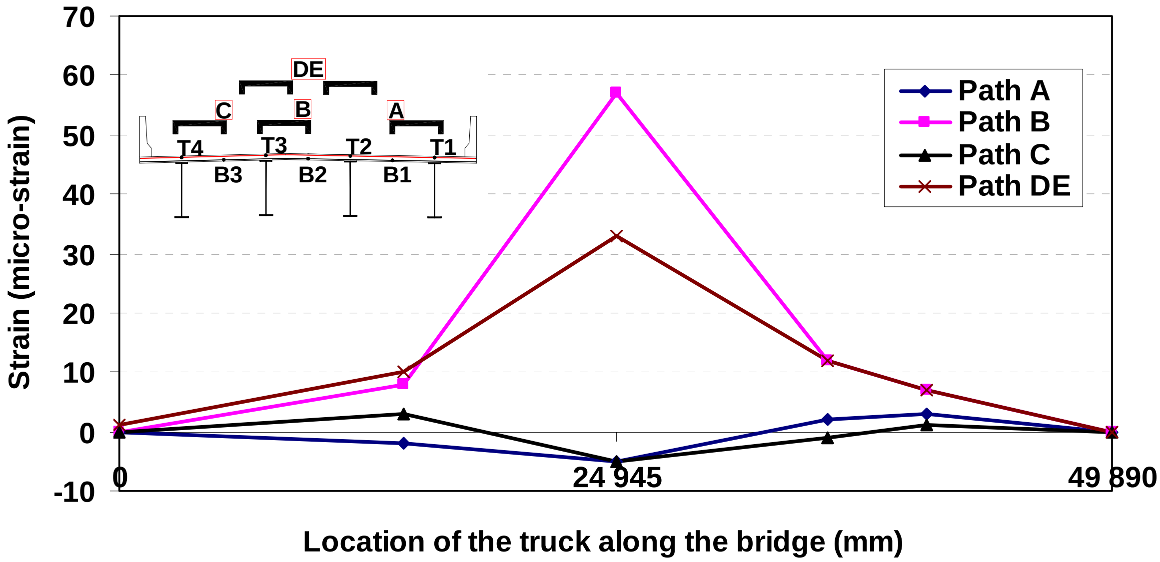

Figure 14 – Measured strains in bottom transverse reinforcement for different paths (Gauge B2)

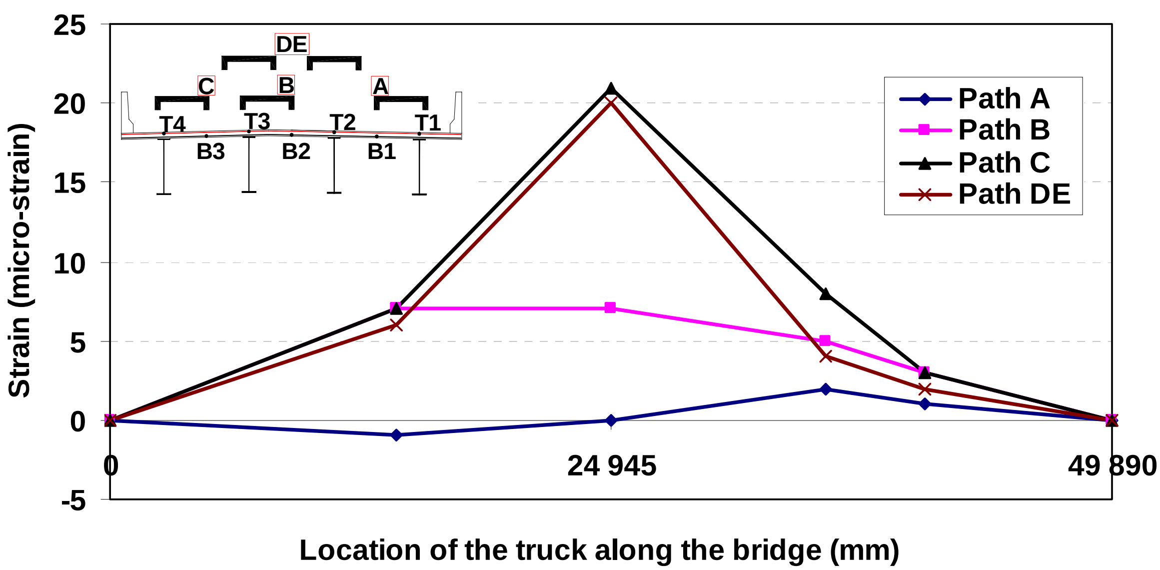

Figure 15 – Measured strains in bottom transverse reinforcement for different paths (Gauge B3)

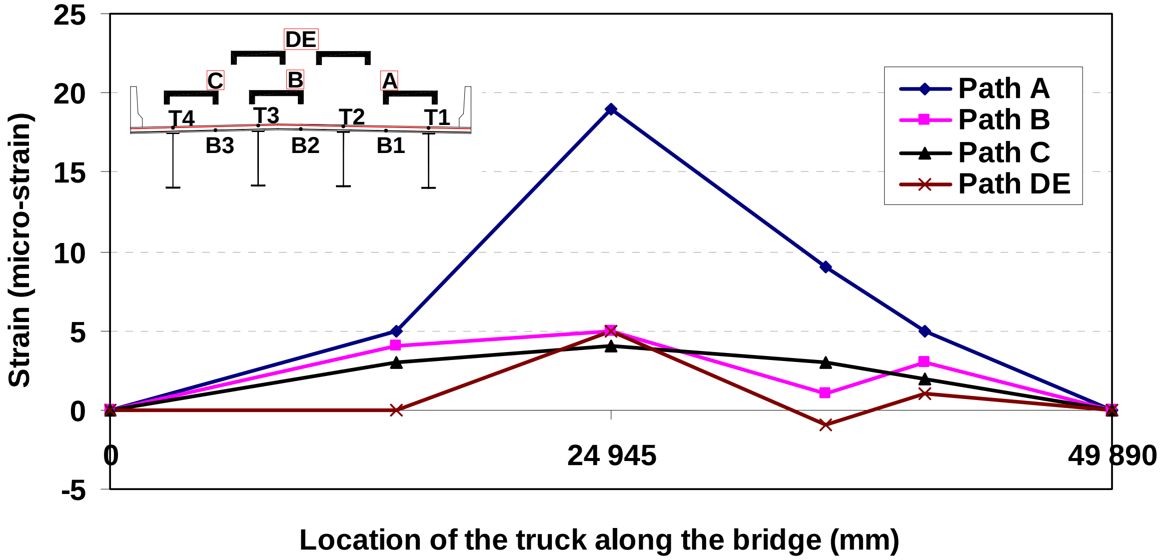

Figure 16 – Measured strains in top transverse reinforcement for different paths (Gauge T1)

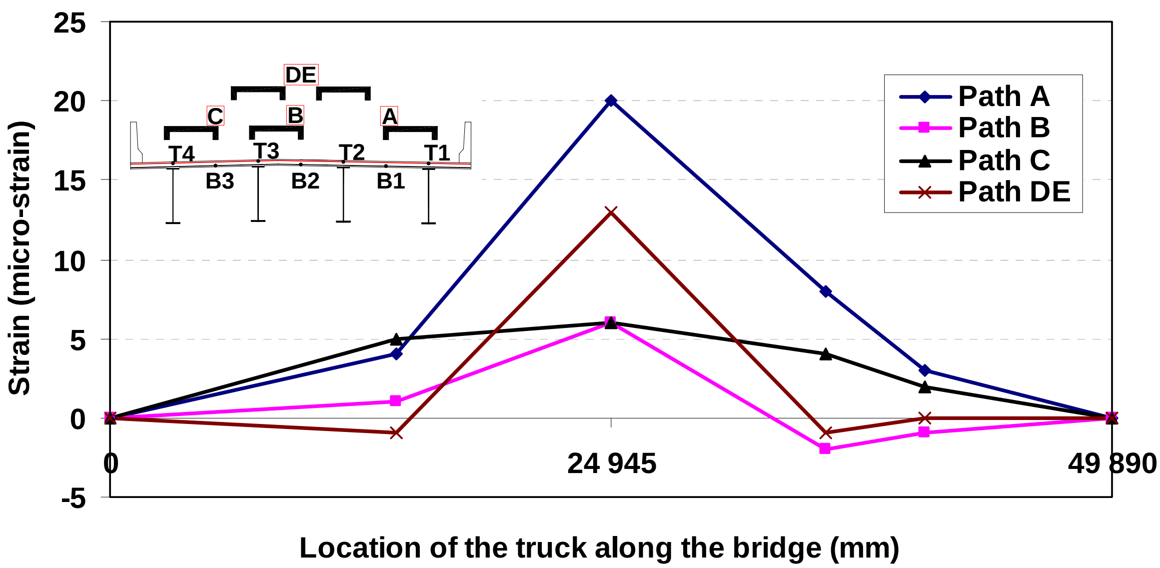

Figure 17 – Measured strains in top transverse reinforcement for different paths (Gauge T2)

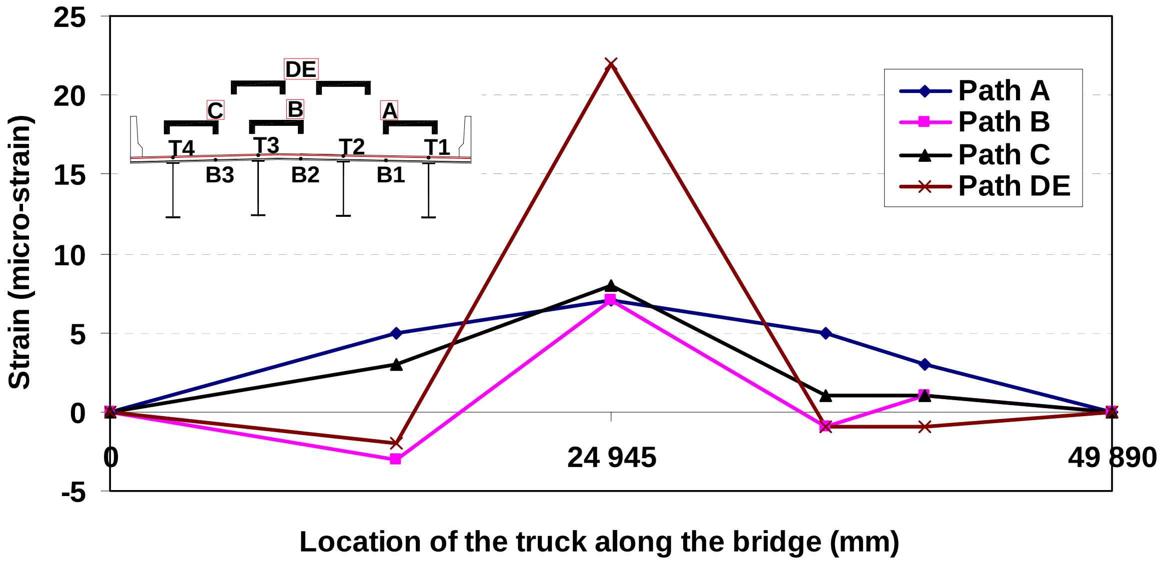

Figure 18 – Measured strains in top transverse reinforcement for different paths (Gauge T3)

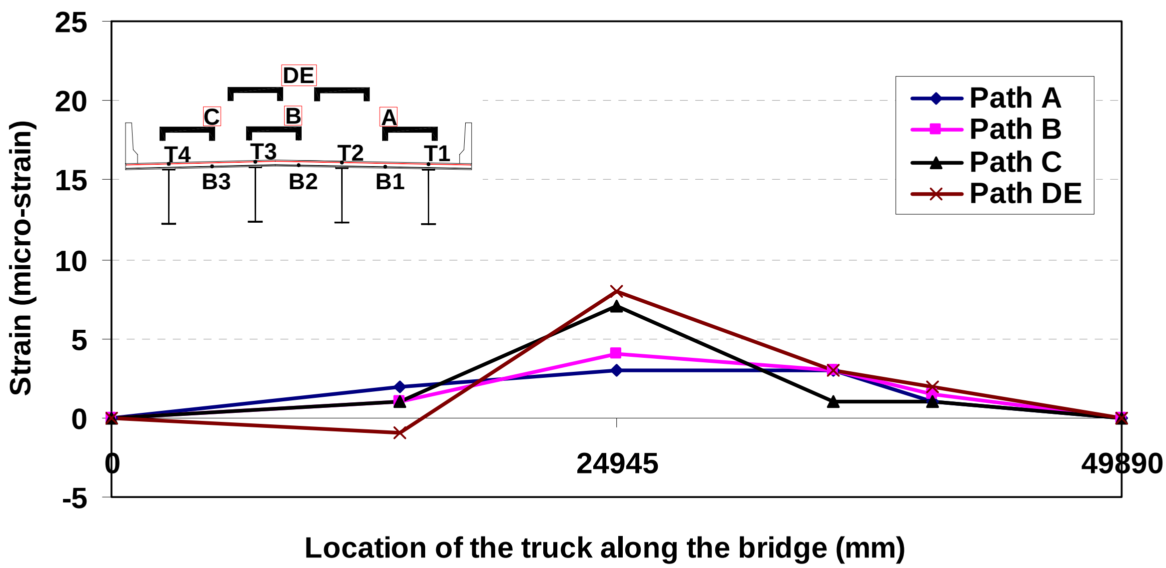

Figure 19 – Measured strains in top transverse reinforcement for different paths (Gauge T4)

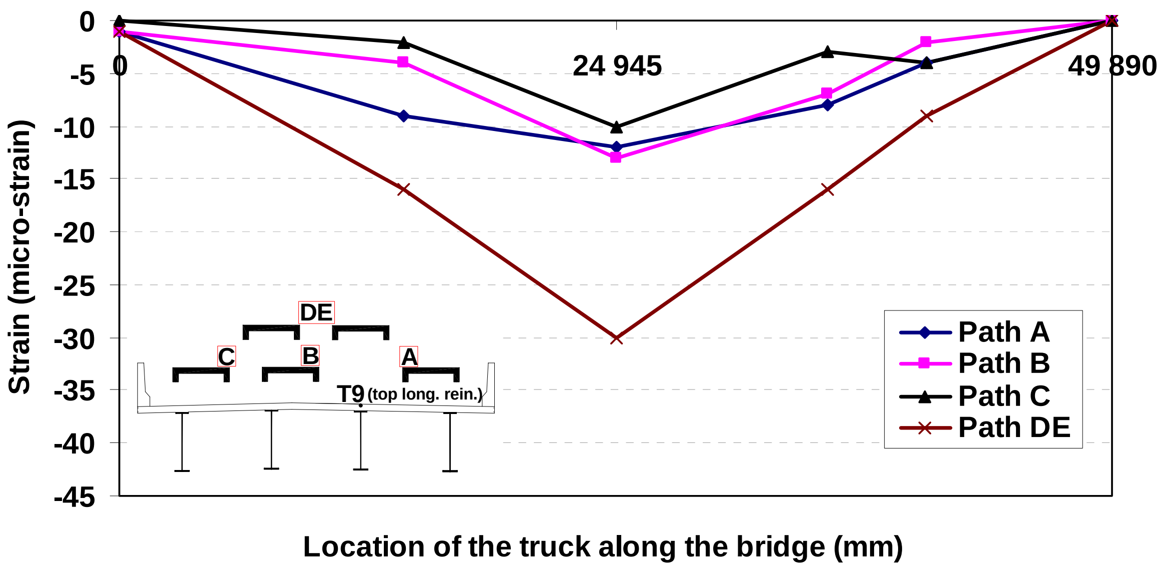

Figure 20 – Measured strains in top longitudinal reinforcement for different paths (Gauge T9)

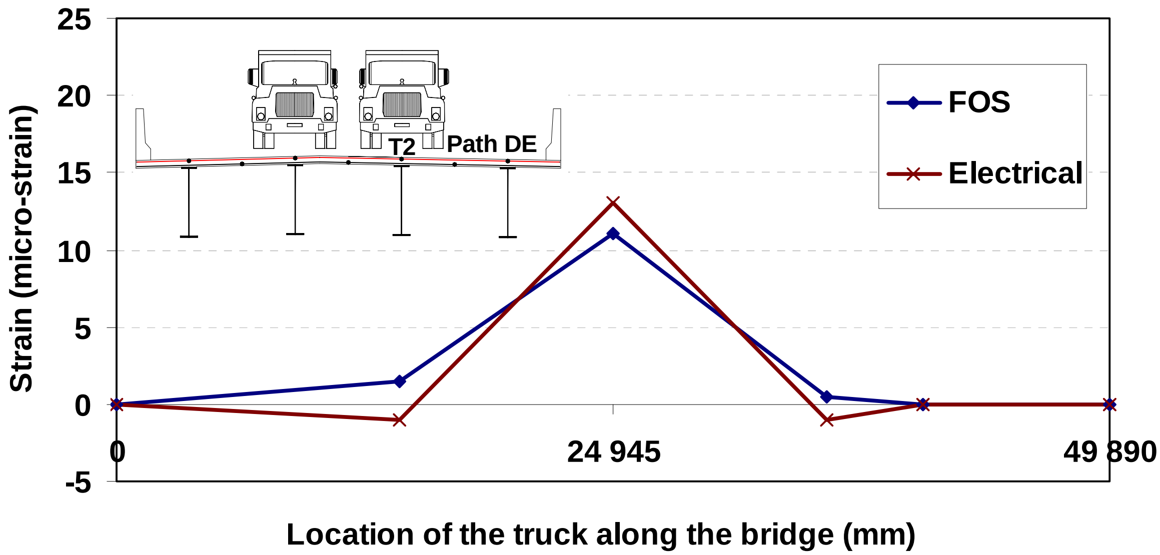

Figure 21 – Comparison between FOS and electrical strain gauge reading (Gauge T2, two trucks on path DE)

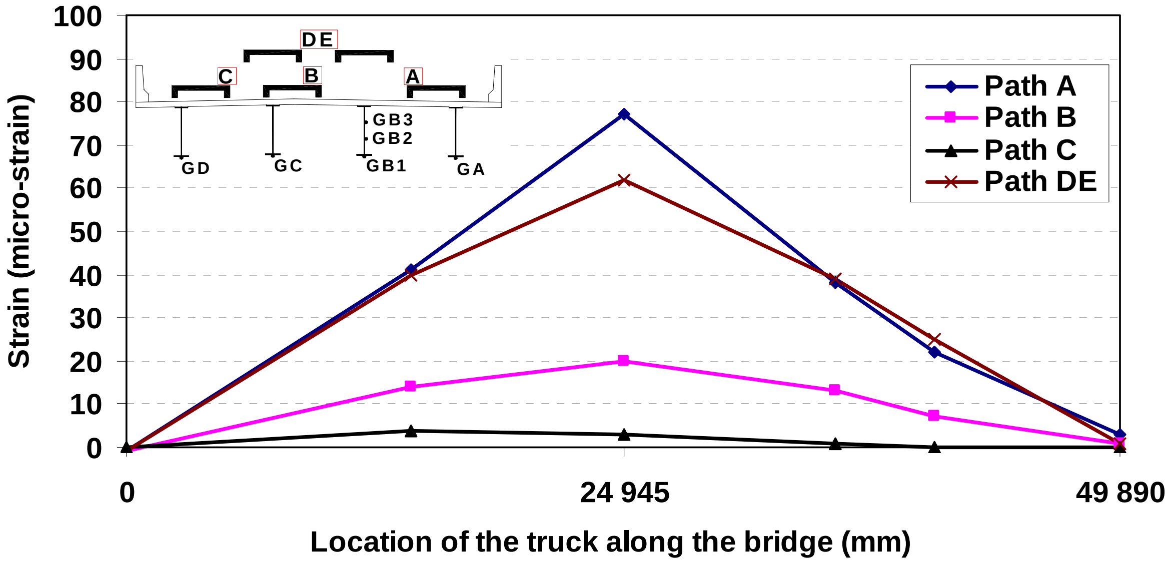

Figure 22 – Measured strains in the bottom flange of girder A for different paths (Gauge GA)

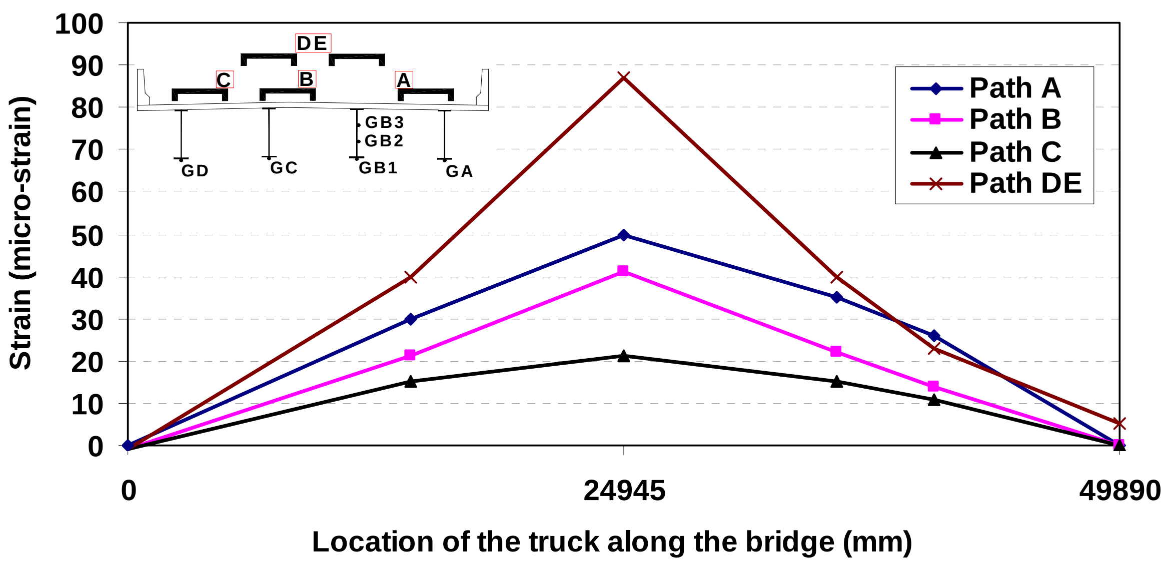

Figure 23 – Measured strains in the bottom flange of girder B for different paths (Gauge GB1)

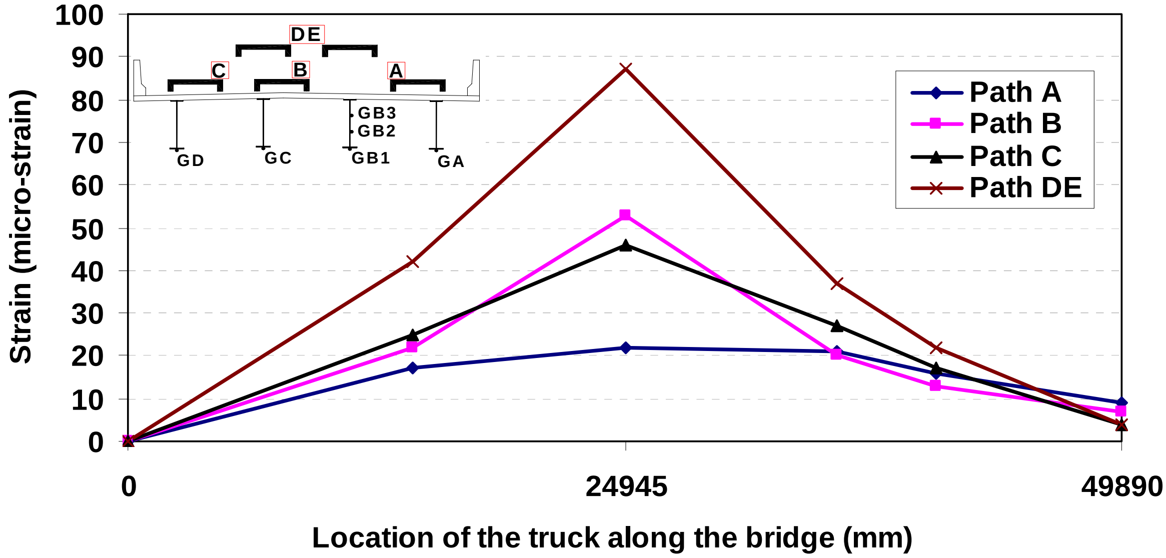

Figure 24 – Measured strains in the bottom flange of girder C for different paths (Gauge GC)

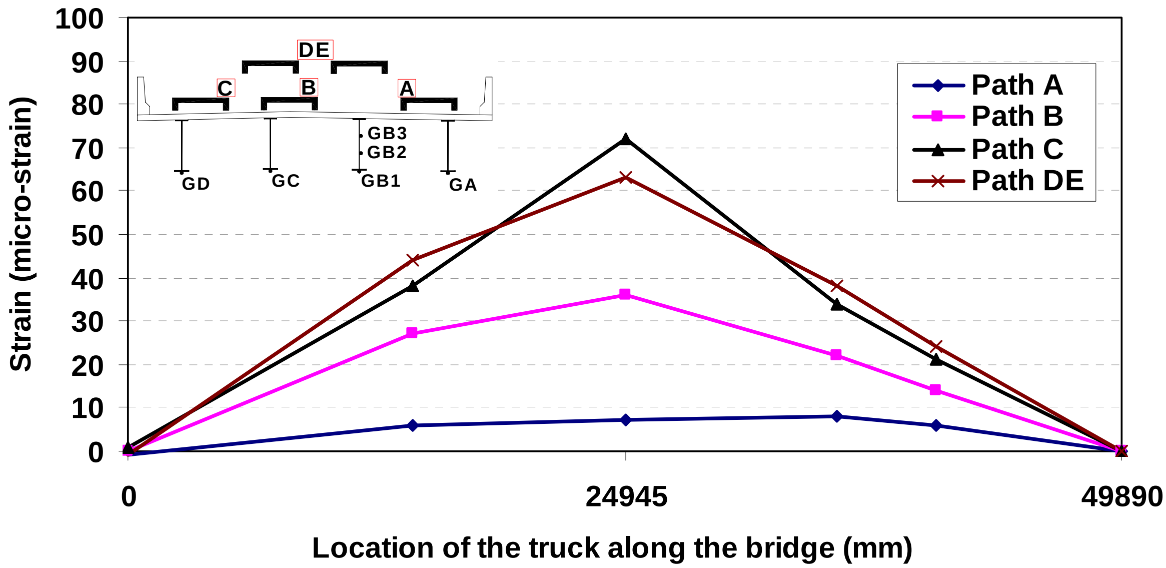

Figure 25 – Measured strains in the bottom flange of girder D for different paths (Gauge GD)

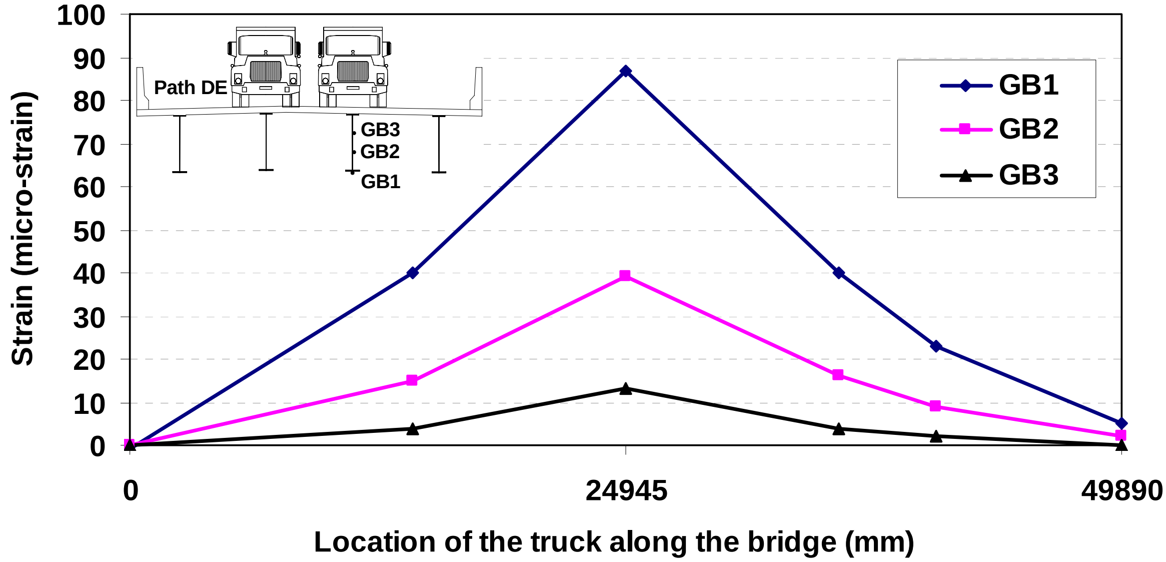

Figure 26 – Comparison between strains at the bottom flange and at the web of girder B (path DE)

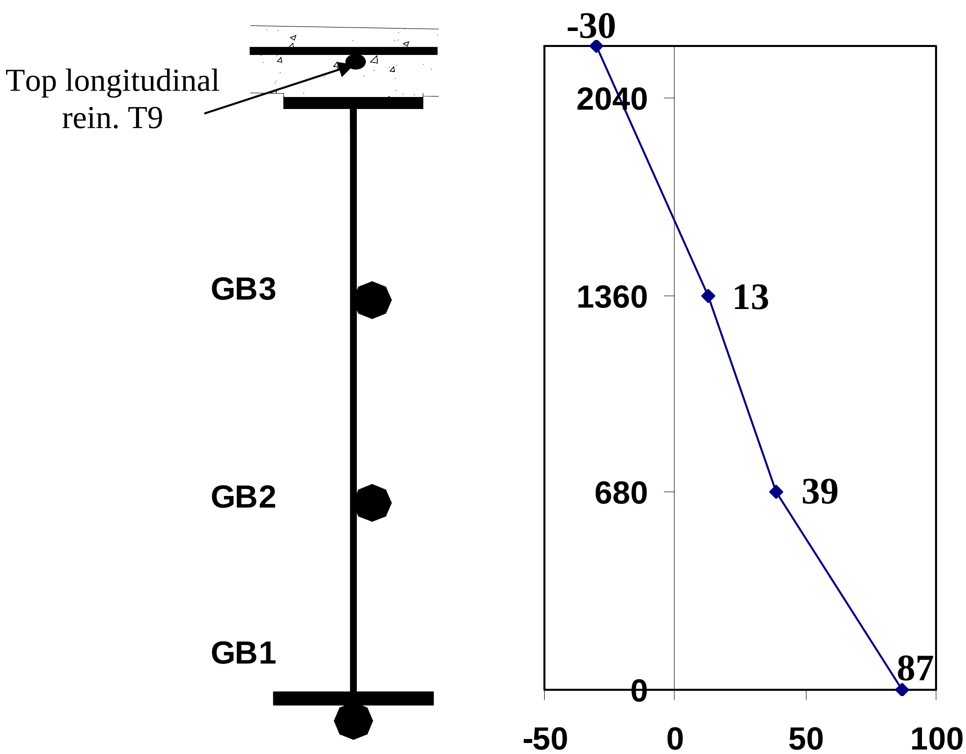

Figure 27 – Strain distribution for Girder C (Path DE)

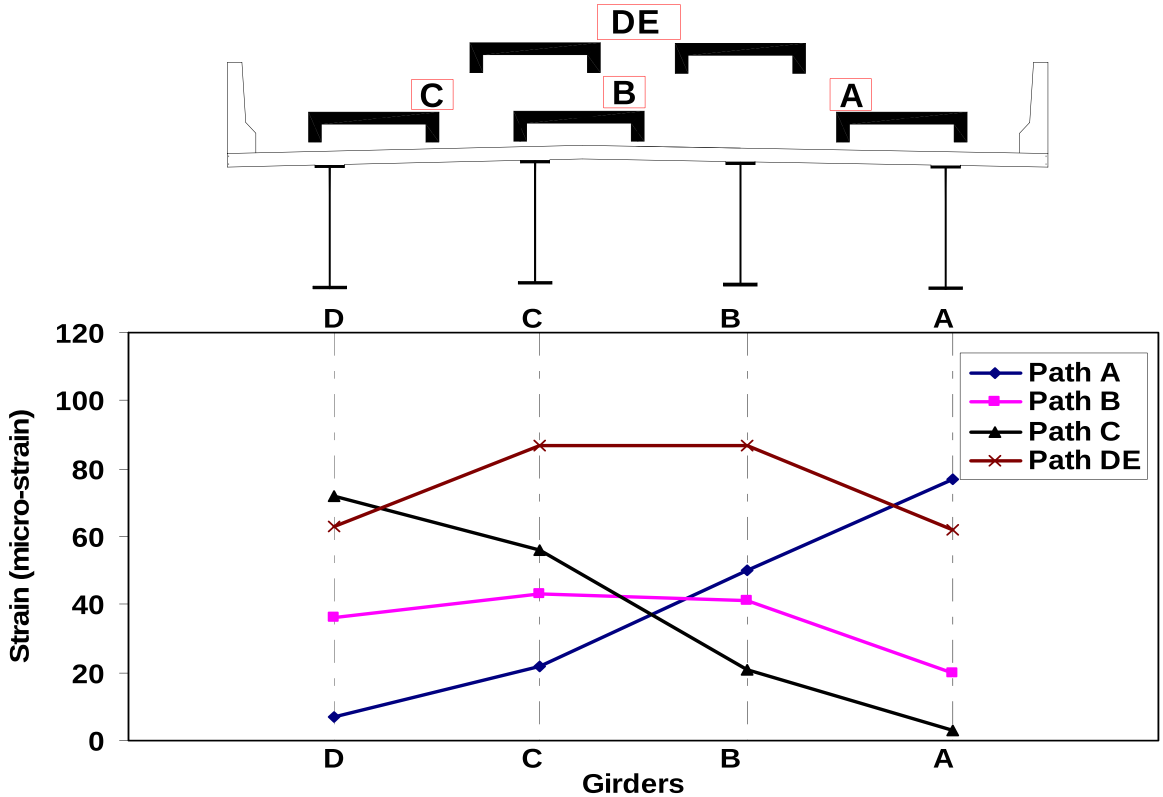

Figure 28 – Distribution of maximum strains in steel girders (truck load at section 1)

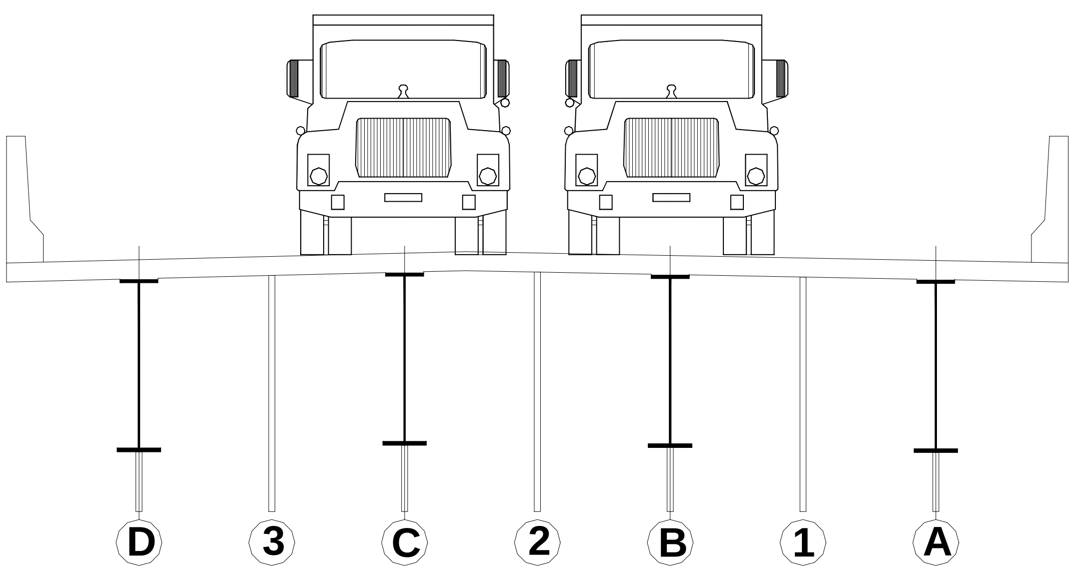

Figure 29 – Schematic drawing for the locations of deflection rulers (section 1, at the mid span of the bridge)

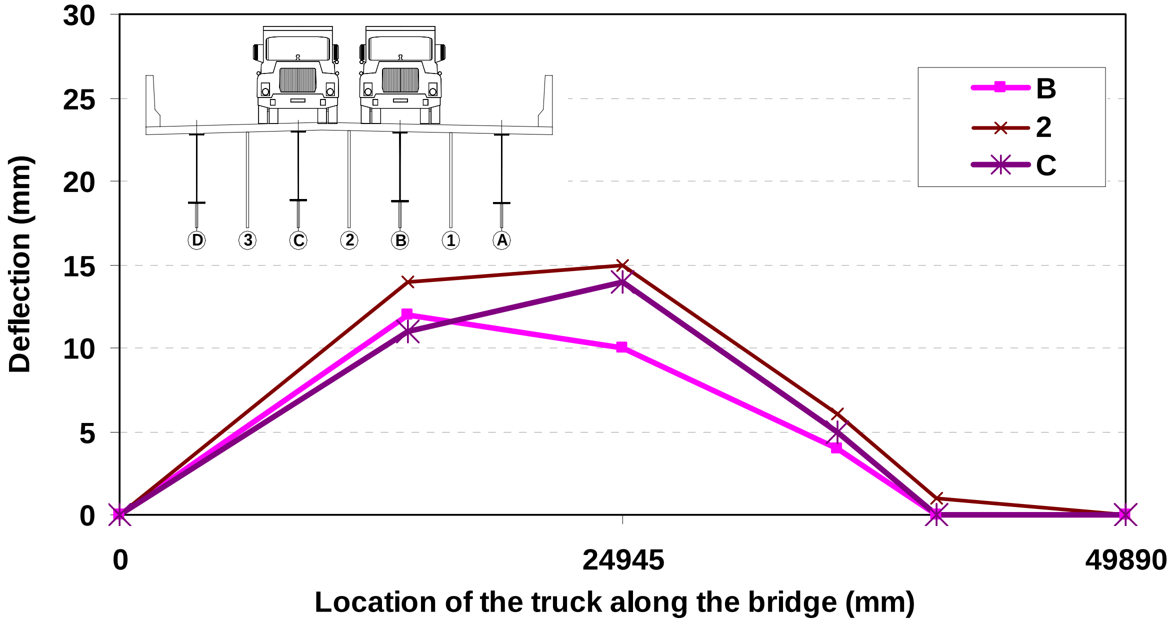

Figure 30 – Measured deflections in rulers B, 2, and C (Path DE)

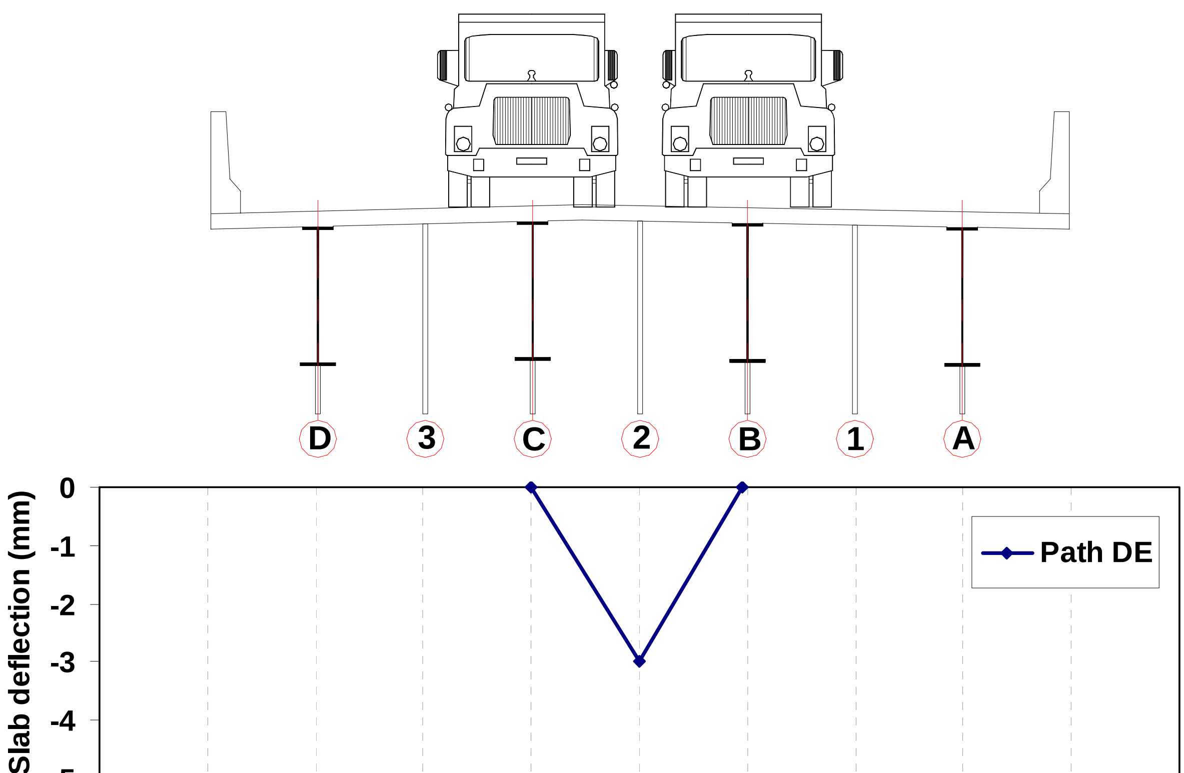

Figure 31 – Maximum measured deflections at mid span (Path DE)

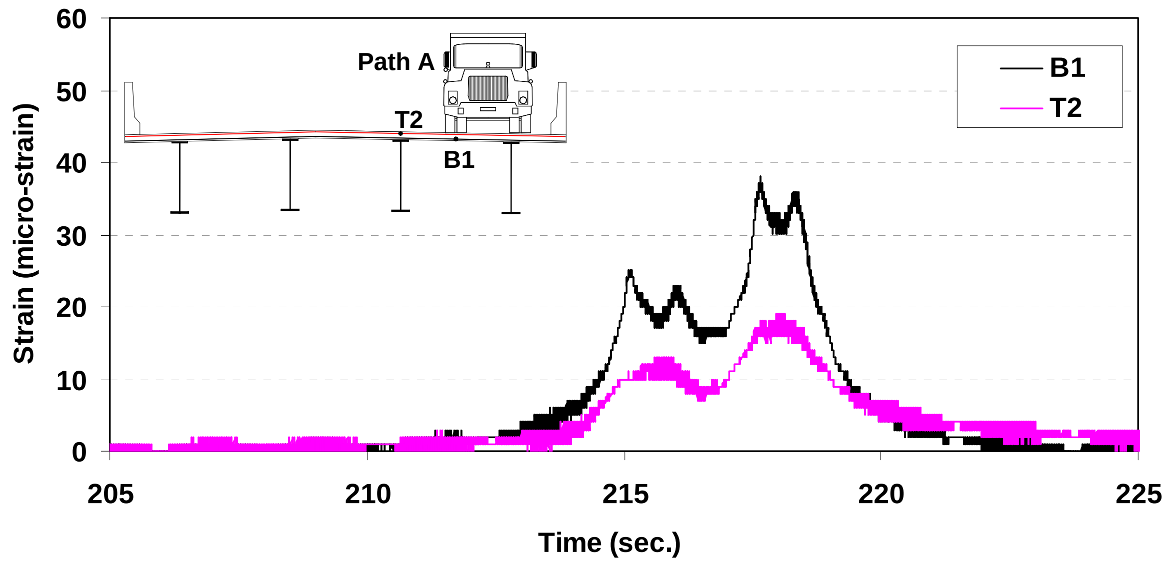

Figure 32 – Maximum tensile strains in top and bottom FRP bars (Gauges B1 and T2)
(One truck traveling over Path A - 5 km/hr.)

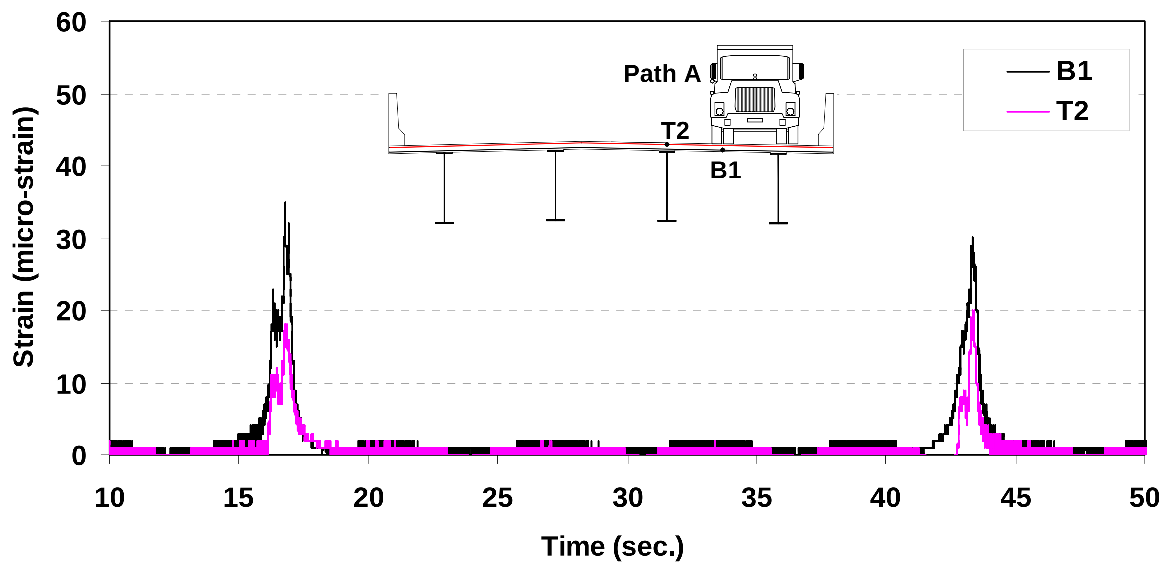

Figure 33 – Maximum tensile strains in top and bottom FRP bars (Gauges B1 and T2)
(Two truck traveling simultaneously over Path A - 50 km/hr.)

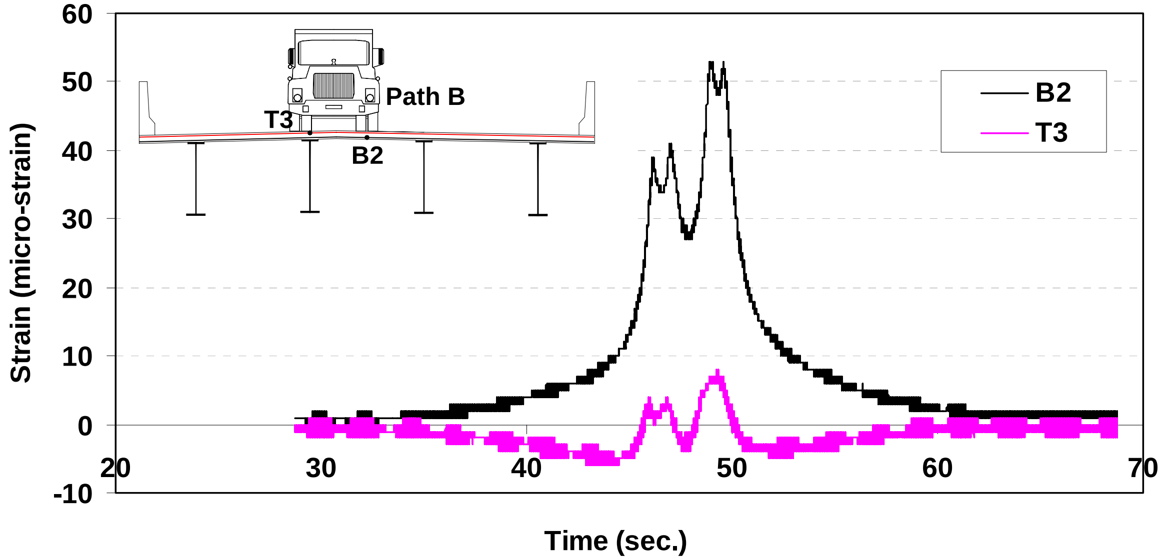

Figure 34 – Maximum tensile strains in top and bottom FRP bars (Gauges B2 and T3)
(One truck traveling over Path B - 5 km/hr.)

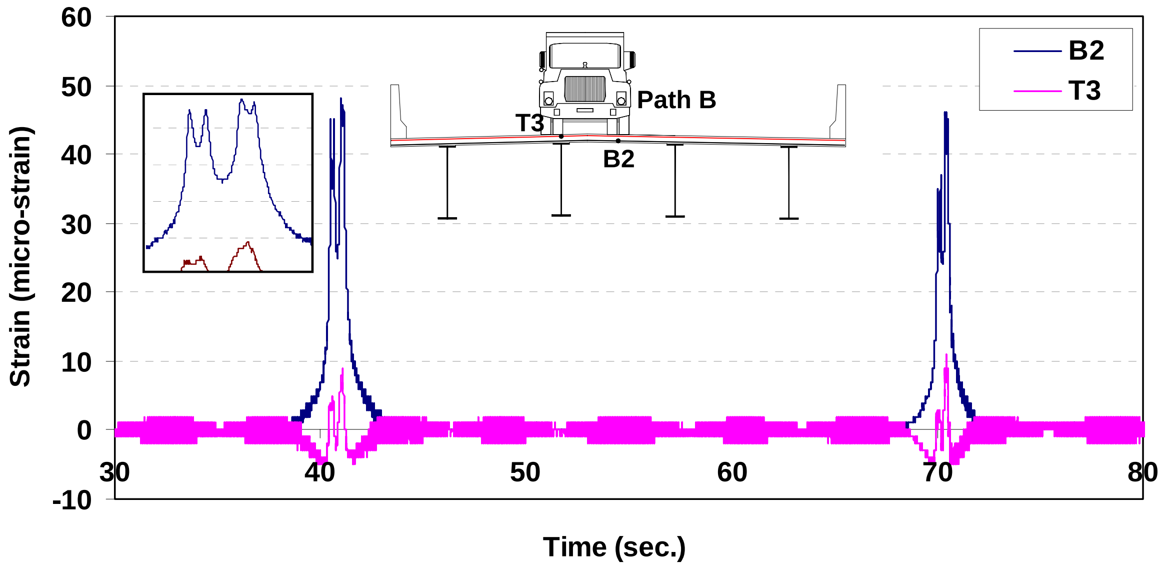

Figure 35 – Maximum tensile strains in top and bottom FRP bars (Gauges B2 and T3)
(Two truck traveling simultaneously over Path B - 50 km/hr.)

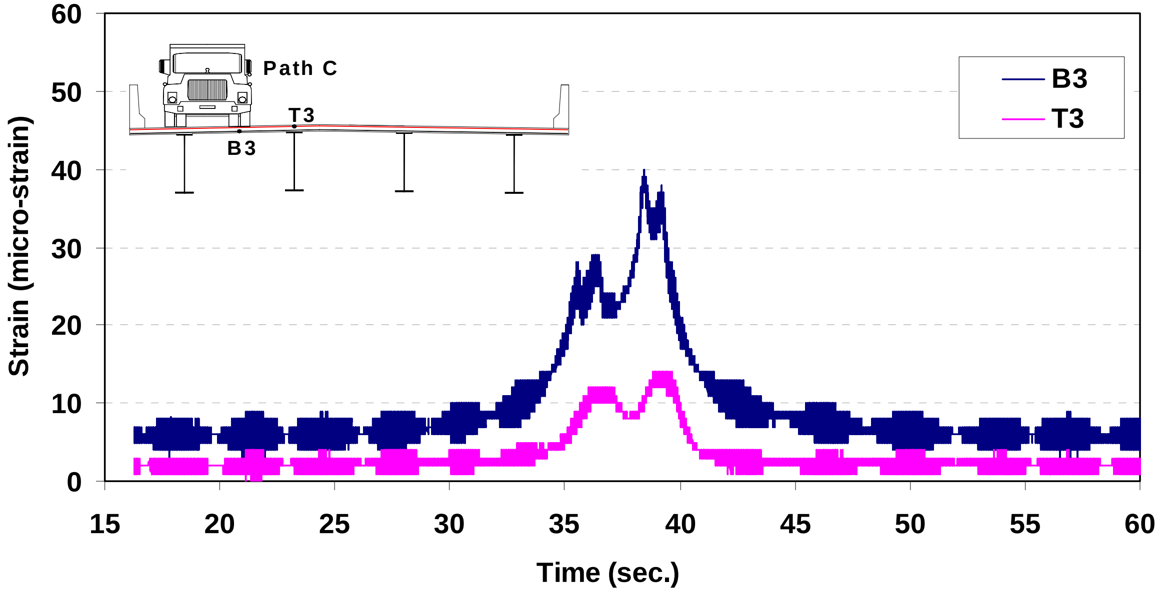

Figure 36 – Maximum tensile strains in top and bottom FRP bars (Gauges B3 and T3)
(One truck traveling over Path C - 5 km/hr.)

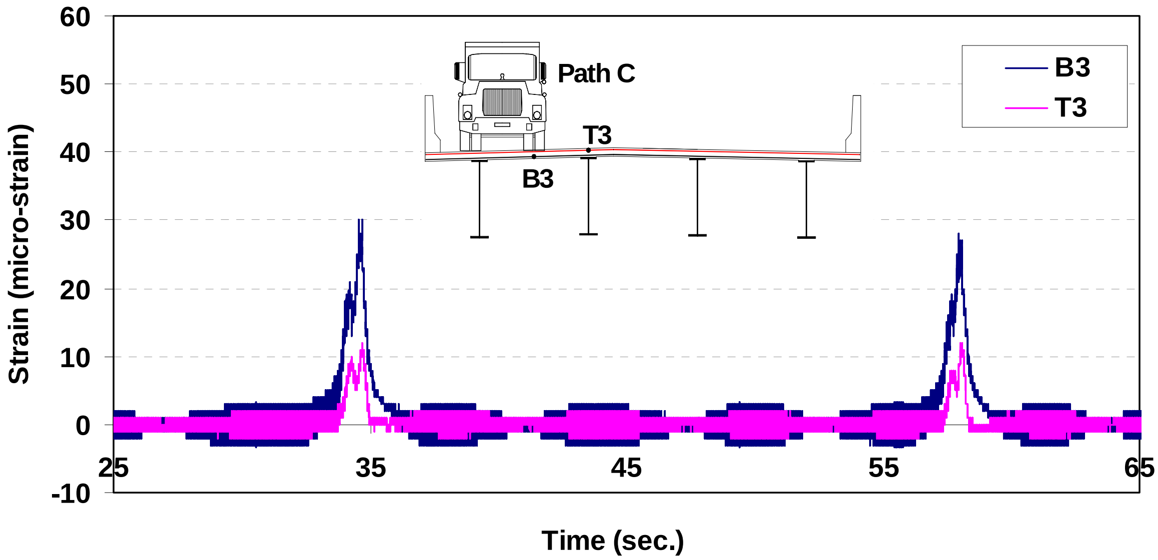

Figure 37 – Maximum tensile strains in top and bottom FRP bars (Gauges B2 and T3)
(Two truck traveling simultaneously over Path C - 50 km/hr.)

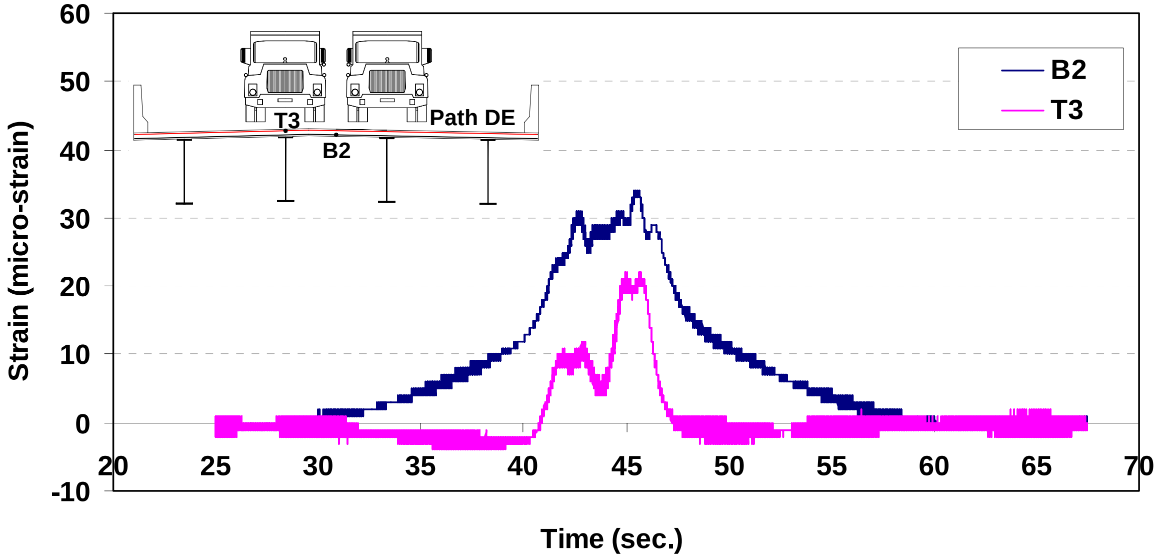

Figure 38 – Maximum tensile strains in top and bottom FRP bars (Gauges B2 and T3)
(Two trucks beside each other traveling over Path DE - 5 km/hr.)

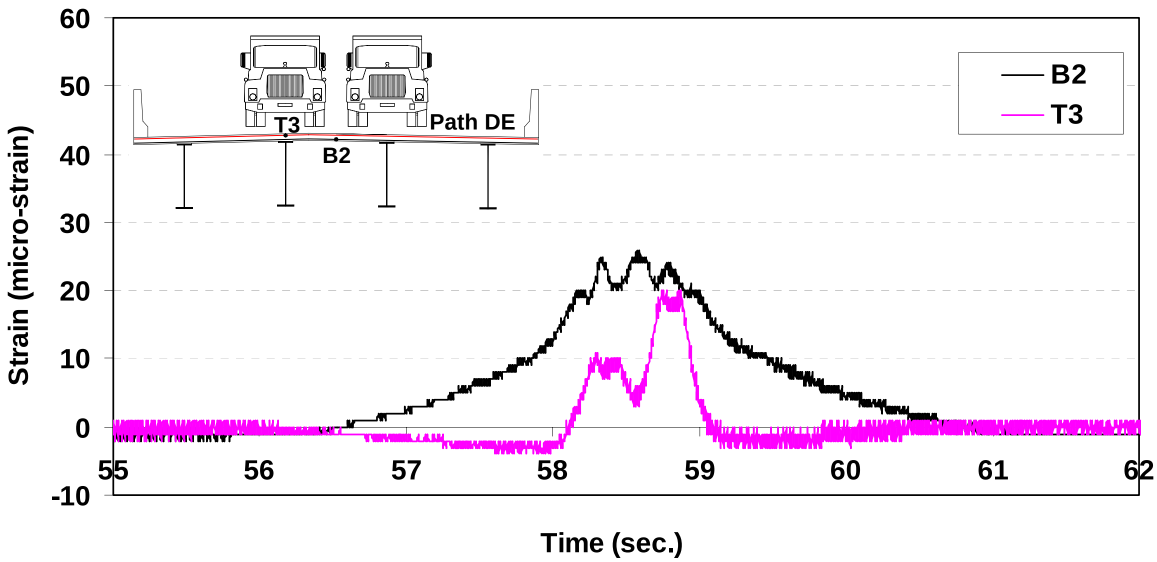

Figure 39 – Maximum tensile strains in top and bottom FRP bars (Gauges B2 and T3)
(Two trucks beside each other traveling over Path DE - 50 km/hr.)

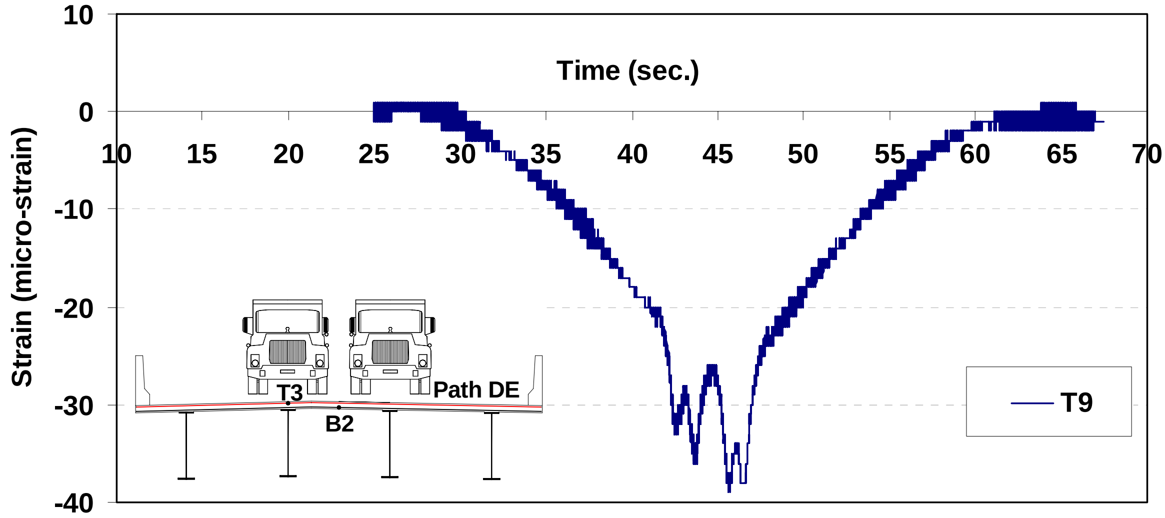

Figure 40 – Maximum compressive strains in top FRP bars (Gauge T9)

(Two truck over Path DE - 5 km/hr.)

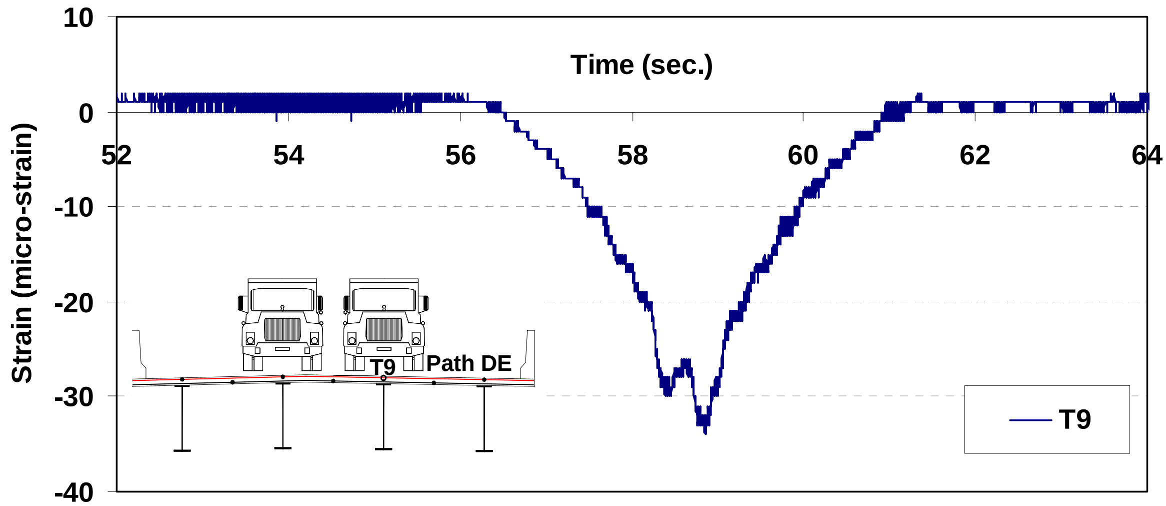

Figure 41 – Maximum compressive strains in top FRP bars (Gauge T9)

(Two truck over Path DE - 50 km/hr.)

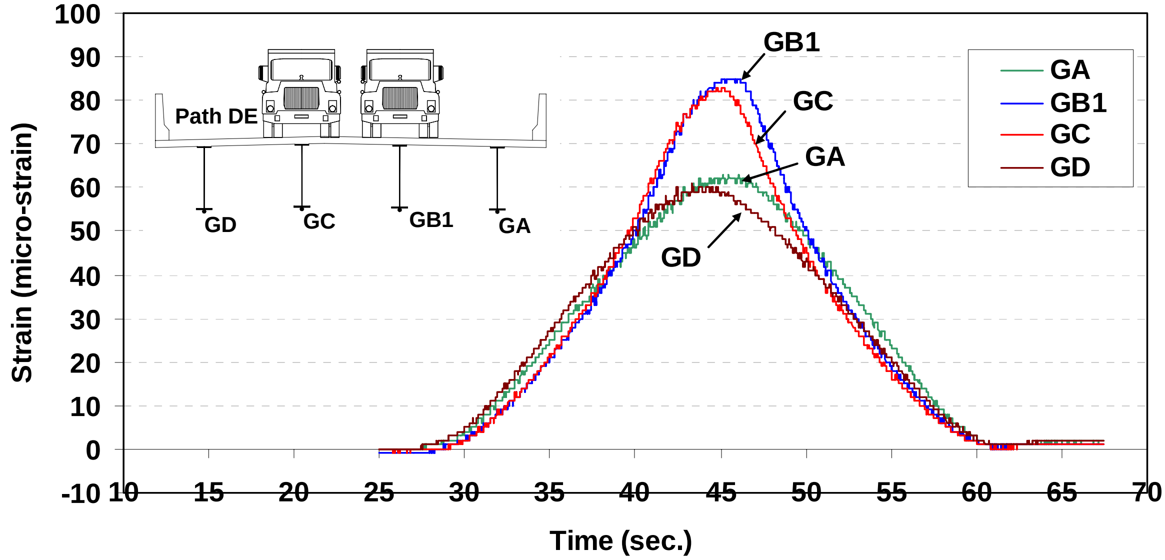

Figure 42 – Maximum tensile strains in the bottom flange of the steel girders

(Two trucks beside each other traveling over Path DE - 5 km/hr.)

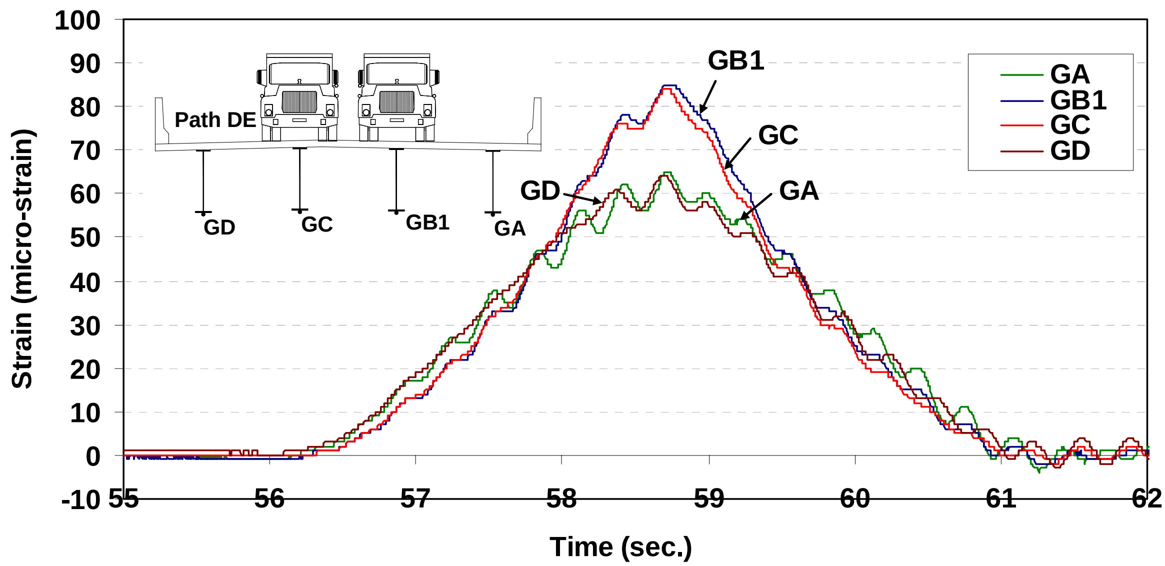

Figure 43 – Maximum tensile strains in the bottom flange of the steel girders

(Two truck over Path DE - 50 km/hr.)